Table I. Echocardiographic and hemodynamic analysis at 8 or 20 weeks of age

	8 weeks		20 weeks	
	NTg	Tg	NTg	Tg
Echocardiographic data	$n = 6$	$n = 6$	$n = 5$	$n = 5$
LVDd (mm)	4.02 ± 0.11	4.00 ± 0.29	4.04 ± 0.23	5.32 ± 0.22[a]
LVDs (mm)	2.76 ± 0.14	2.87 ± 0.20	2.58 ± 0.15	4.66 ± 0.15[a]
IVST (mm)	0.66 ± 0.038	0.65 ± 0.028	0.58 ± 0.08	0.60 ± 0.06
PWT (MM)	0.67 ± 0.042	0.69 ± 0.034	0.60 ± 0.07	0.54 ± 0.05
FS (%)	32.8 ± 1.88	27.9 ± 1.54	36.2 ± 2.08	12.0 ± 0.84[a]
EF (%)	69.7 ± 2.56	62.67 ± 2.20	71.8 ± 2.75	30.4 ± 1.94
Hemodynamic data	$n = 4$	$n = 5$	$n = 6$	$n = 5$
dP/dt_{max} (mmHg/s)	4865 ± 201	4757 ± 325	4090 ± 188	2328 ± 264[a]
dP/dt_{min} (mmHg/s)	−4935 ± 218	−4756 ± 237	−4150 ± 193	−2264 ± 292[a]
HR (/min)	498 ± 26.9	533 ± 29.4	503 ± 42.8	487 ± 43.6
LVSP (mmHg)	98.9 ± 4.53	95.1 ± 3.6	88.4 ± 3.54	68.3 ± 5.34[a]
LVEDP (mmHg)	2.25 ± 0.56	2.36 ± 0.69	3.83 ± 1.04	7.68 ± 2.30

Values are means ± SEM. LVDd, left ventricular end diastolic dimension; LVDs, left ventricular end systolic dimension; IVST, interventricular septal thickness; PWT, posterior wall thickness; FS, fractional shortening; EF, ejection fraction; dP/dt, first derivative of pressure; HR, heart rate; LVSP, left ventricular systolic pressure; LVEDP, left ventricular end diastolic pressure.
[a]$P < 0.05$ dnNRSF Tg versus NTg mice.

α-MHC promoter (Figure 1B). Two independently derived dnNRSF transgenic (Tg) founders (Tg471 and Tg474; *dnNRSF* mRNAs were expressed at levels 35.5- and 27.0-fold higher than endogenous *NRSF* mRNAs, respectively) were obtained and investigated (Figure 1C). The data obtained from Tg471, which are essentially identical to those obtained from Tg474, are presented below. Western blot analysis confirmed that expression of dnNRSF was restricted to the heart, though weak expression was observed in the lung, where endogenous α-*MHC* is expressed in cardiac myocytes surrounding pulmonary veins (Figure 1D) (Subramaniam *et al.*, 1991).

To determine the role of NRSF in the regulation of fetal cardiac gene expression *in vivo*, we carried out northern blot analyses of the genes for ANP, BNP, α-skeletal actin, β-MHC, α-cardiac actin, myosin light chain (MLC)-2v, sarcoplasmic/endoplasmic reticulum Ca^{2+} ATPase (SERCA) 2 and GAPDH using total RNA prepared from ventricles taken from 8- and 20-week-old mice (Figure 1E and F). The expression of the genes for ANP, BNP and α-skeletal actin, which contain an NRSE, was selectively upregulated in the hearts of dnNRSF Tg mice by 8 weeks of age. In 8-week-old dnNRSF Tg and non-transgenic (NTg) mice, the expression of another fetal gene, β-*MHC*, which does not contain an NRSE, was not enhanced, and the heart to body weight ratios and cardiac function estimated by echocardiography and hemodynamic analysis were not different. Apparently, induction of these fetal genes in 8-week-old dnNRSF Tg hearts is a primary effect of NRSF inhibition (Figures 1E and F, and 3B and C and Table I). Taken together, these results and the data obtained from *in vitro* studies using cultured ventricular myocytes, which are not affected by hemodynamic alterations, clearly indicate that NRSF regulates expression of multiple fetal cardiac genes in ventricular myocytes.

Several earlier studies reported that expression of *NRSF* mRNA is barely detectable in fetal hearts, though its expression is detected in neonatal ventricular myocytes and adult hearts (Schoenherr and Anderson, 1995; Chong *et al.*, 1995; Palm *et al.*, 1998; Grimes *et al.*, 2000; Kuwahara *et al.*, 2001). We therefore used RT–PCR to examine expression of *NRSF* and *ANP* in fetal ventricles obtained from 13.5-day mouse embryos and adult ventricles from 20-week-old mice. Consistent with those earlier reports, expression of *NRSF* mRNA was significantly lower in the embryonic than adult ventricles. Conversely, expression of *ANP* mRNA was significantly lower in adult ventricles than embryonic ventricles (Figure 1G). These results, which were confirmed by quantitative real-time RT–PCR (Figure 1H), suggest that NRSF plays a role in the developmental regulation of fetal cardiac gene expression and further support the notion that NRSF represses expression of fetal cardiac genes.

NRSF plays an important role in the re-expression of fetal cardiac genes induced by hypertrophic stimuli

To examine further the role of NRSF in the re-expression of endogenous fetal cardiac genes *in vivo*, we subjected the hearts of dnNRSF Tg mice and their NTg littermates to acute pressure overload created by transverse aortic constriction (TAC). As previously reported (Harada *et al.*, 1998), acute pressure overload induced expression of c-*fos* and *BNP* in NTg hearts within 30 min after the onset of TAC (Figure 2A–C). Northern blot analysis showed that basal levels of *BNP* expression were higher in 8-week-old dnNRSF Tg than NTg hearts, but that induction of *BNP* expression by TAC was less pronounced in dnNRSF Tg hearts (Figure 2A and B). In contrast, the inducibility of c-*fos* expression and peak-to-peak systolic pressure gradients across the stenosis were similar in dnNRSF Tg and NTg hearts (Figure 2A, C and D). These results were confirmed by quantitative RT–PCR analysis for *BNP* mRNA expression (Figure 2E) and indicate that *BNP* expression is constitutively elevated in hearts expressing dnNRSF, though its inducibility is diminished.

Consistent with that finding, expression of dnNRSF markedly reduced the fold increases in endogenous *ANP*, *BNP* and α-*skeletal actin* expression induced by ET-1 in

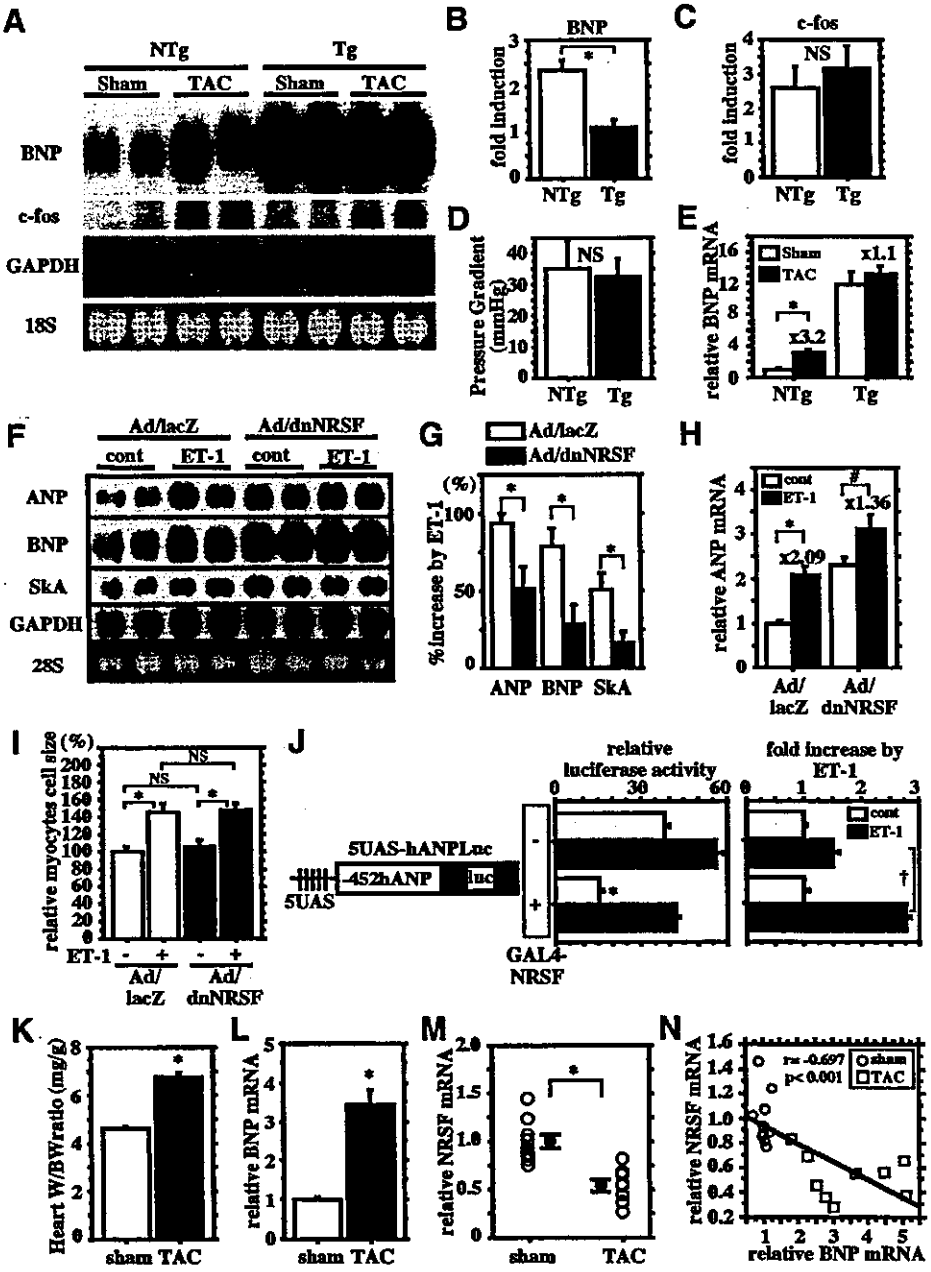

Fig. 2. NRSF regulates the inducible response of cardiac fetal gene expression to hypertrophic stimuli. (A) Northern blots showing levels of *BNP*, c-*fos* and *GAPDH* mRNA in sham- or TAC-operated NTg and dnNRSF Tg hearts. (B and C) Bar graphs summarizing the fold increases in *BNP* (B) and c-*fos* (C) mRNA detected in the northern blots shown in (A); $n = 4$ each. (D and E) Pressure gradients across the stenosis after TAC (D) and quantitative real-time RT–PCR analyses for *BNP* mRNA expression (E); $n = 4$ each. (F) Representative northern blots showing levels of *ANP*, *BNP*, *SkA* and *GAPDH* mRNA in cultured ventricular myocytes infected with Ad/lacZ or Ad/dnNRSF and subsequently treated for 24 h with or without 10 nM ET-1. (G) Bar graphs summarizing the percentage increases in the levels of *ANP*, *BNP* and *SkA* mRNA elicited by 10 nM ET-1 detected in the northern blots shown in (F); $*P < 0.05$ versus Ad/lacZ; $n = 5$ each. (H) Bar graph summarizing the results of a quantitative real-time RT–PCR analysis of *ANP* mRNA expression; $*P < 0.01$, $P < 0.05$; $n = 4$ each. The numbers above each bar indicate the fold increase induced by ET-1. For (B), (C), (E), (G) and (H), relative mRNA levels (normalized to *GAPDH* mRNA levels) are presented as means ± SEM. (I) Surface areas of 40 randomly selected cells in each group normalized to control myocytes (=100%) (mean ± SEM); $*P < 0.05$; NS, not significant. (J) The promoter activities of 5UAS-hANPLuc in ventricular myocytes treated or not with 10 nM ET-1 for 48 h in the absence or presence of a GAL4-NRSF fusion protein. The activities of the construct transfected into myocytes treated with 10 nM ET-1 are expressed as the fold increase over the value for myocytes treated without ET-1 in the right panel. Bars represent means ± SEM of the relative luciferase activity from at least three separate assays carried out in triplicate; $*P < 0.05$ versus GAL4-NRSF(–) ET-1(–); $\dagger P < 0.05$. (K) Heart weight to body weight ratios in sham- and TAC-operated mice. Bars represent means ± SEM. (L and M) Quantitative RT–PCR analysis of *BNP* (L) and *NRSF* (M) mRNA levels. Relative mRNA levels (normalized to *GAPDH* mRNA levels) are presented as means ± SEM; levels in sham-operated mice are assigned a value of 1.0; $*P < 0.05$ versus sham-operated mice. (N) Inverse correlation between expression of ventricular *BNP* and *NRSF* mRNAs.

cultured ventricular myocytes (Figure 2F–H), whereas it had no significant effect on ET-1-induced increases in cell size (Figure 2I). In addition, when we incubated ventricular myocytes co-transfected with an *ANP* promoter–reporter construct containing GAL4-binding sites (5UAS-hANPLuc) and a plasmid encoding a GAL4 DNA-binding domain–NRSF fusion protein (GAL4-NRSF) with ET-1, we found that in the presence of

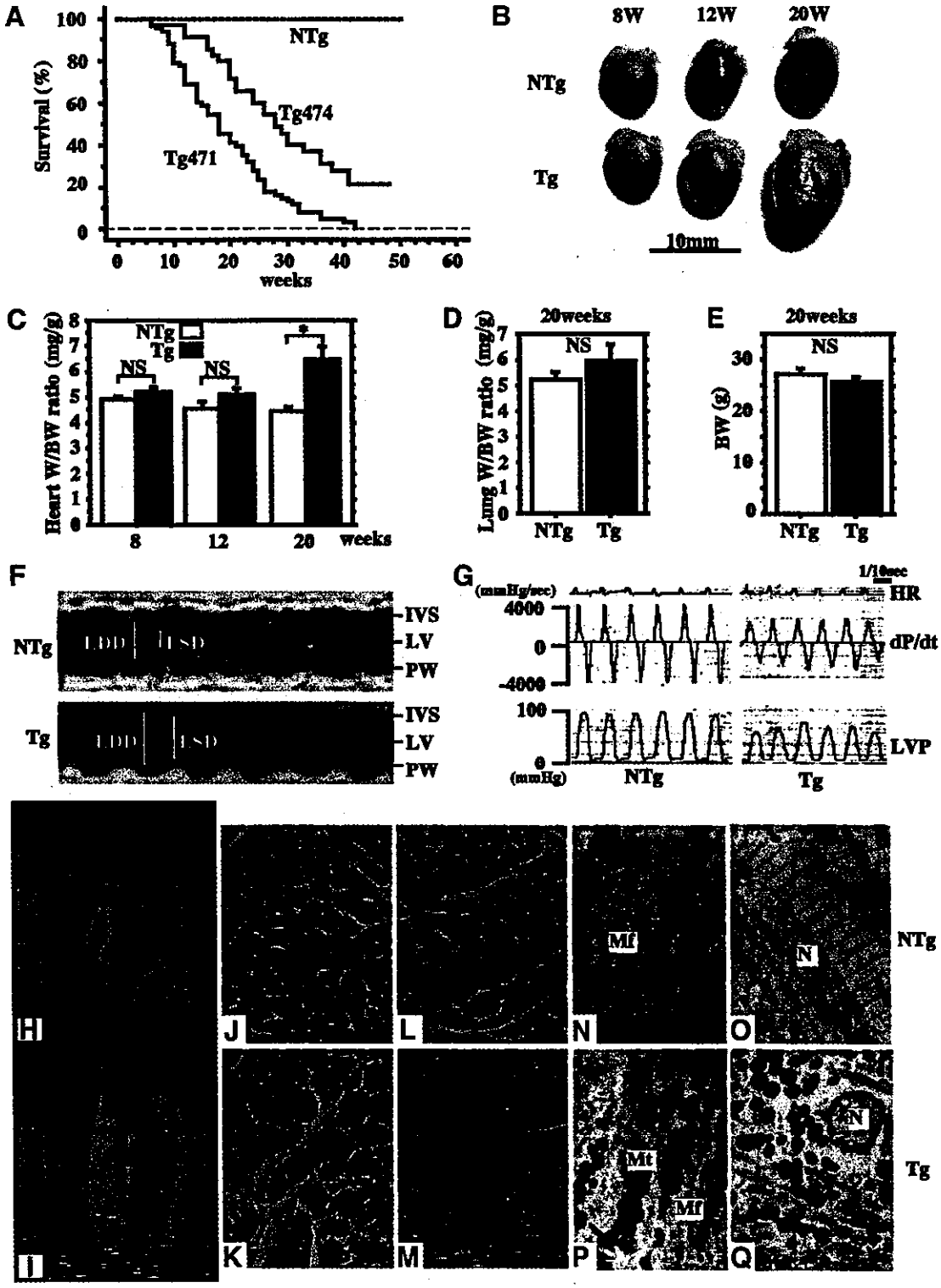

Fig. 3. Dilated cardiomyopathy in dnNRSF Tg mice. (A) Kaplan–Meier survival analysis of dnNRSF Tg471 (n = 68), Tg474 (n = 35) and NTg (n = 145) mice showing a significant difference in survival rates between dnNRSF Tg and NTg mice (log rank test; $P < 0.0001$). (B) Hearts of NTg and dnNRSF Tg mice at 8, 12 and 20 weeks; scale bars, 10 mm. (C) Heart to body weight ratios (mg/g), (D) lung to body weight ratios (mg/g) and (E) body weights (g) in NTg and dnNRSF Tg mice measured at the indicated times; $*P < 0.05$; NS, not significant. (F) Representative M-mode echocardiographic tracings from 20-week-old NTg and dnNRSF Tg mice: IVS, interventricular septum; LV; left ventricle; PW, posterior wall; ESD, end systolic dimension; EDD, end diastolic dimension. (G) Representative high fidelity left ventricular pressure tracings from 20-week-old NTg and dnNRSF Tg mice: HR, heart rate; LVP, LV pressure. (H–Q) Histological analysis of hearts from 20-week-old NTg and dnNRSF Tg mice. (H and I) Hearts from NTg (H) and dnNRSF Tg (I) mice were sectioned longitudinally and stained with HE; scale bars, 2.5 mm. (J–M) Photomicrographs of histological sections of left ventricle from NTg (J and L) and dnNRSF Tg mice (K and M) stained with Masson's trichrome stain; collagen stains blue with trichrome stain (M); scale bars, 20 μm. (N–Q) Transmission electron micrographs of cardiac myocytes from 20-week-old NTg (N and O) and dnNRSF Tg (P and Q) mice: arrows indicate disrupted mitochondria; My, myofibrils; Mt, mitochondria; N, nucleus; scale bars, 1 μm.

GAL4-NRSF, the response of 5UAS-hANPLuc to ET-1 was significantly increased, though the basal control activity of 5UAS-hANPLuc was significantly reduced (Figure 2J). This means that NRSF-mediated repression is necessary for full induction of fetal cardiac gene expression during cardiac muscle cell hypertrophy, which suggests that NRSF contributes not only to the determination of basal expression of fetal cardiac genes but also to the increase in transcriptional efficiency of fetal cardiac genes induced by hypertrophic stimuli.

We next examined cardiac *NRSF* expression in a mouse model of chronic pressure overload-induced left ventricular hypertrophy created by TAC. In mice subjected to TAC for 2 weeks, heart to body weight ratios and ventricular *BNP* expression were significantly higher than in sham-operated mice (Figure 2K and L), whereas *NRSF* mRNA expression was significantly lower in TAC hearts than in control sham-operated hearts (Figure 2M), i.e. ventricular expression of *NRSF* mRNA showed a significant inverse correlation with ventricular expression of *BNP* mRNA (Figure 2N). Collectively, these lines of data indicate an involvement of NRSF in molecular pathways leading to the upregulation of fetal gene expression during cardiac hypertrophy and support the idea that release of NRSF-mediated repression contributes to the reinduction of fetal cardiac genes.

Inhibition of NRSF in ventricular myocytes leads to increased mortality and dilated cardiomyopathy in vivo

Persistent inhibition of NRSF had a marked effect on cardiac structure and function. dnNRSF Tg mice started to die by 8 weeks of age, and by 40 weeks 70–95% had died. In contrast, 100% of their NTg littermates remained alive (Figure 3A). Gross examination revealed the hearts of 20-week-old dnNRSF Tg mice to be much larger than those of NTg mice, despite the fact that at 8 weeks of age there is no significant difference in heart size (Figure 3B). The heart to body weight ratios in 8- and 12-week-old dnNRSF Tg and NTg mice were also not significantly different, but by 20 weeks the ratio in dnNRSF Tg mice was 1.48-fold higher than in NTg mice (Figure 3C). Consistent with these data, at 20 weeks of age, β-*MHC* expression was upregulated and *SERCA2* expression was downregulated in dnNRSF Tg hearts as compared with NTg hearts, whereas their expression was unchanged in both mouse types at 8 weeks of age (Figure 1E and F). The manner in which dnNRSF Tg mice died was characterized as sudden death; they were unexpectedly found dead within 24 h of displaying apparently normal behavior and levels of activity. Consistent with this diagnosis, body weights and lung to body weight ratios were not different between NTg and dnNRSF Tg mice, even at 20 weeks of age (Figure 3D and E), and there were no apparent signs of lung or liver congestion (data not shown).

To understand better the changes in the hearts of dnNRSF Tg mice, we carried out a series of detailed echocardiographic, hemodynamic and histological analyses. Two-dimensionally targeted M-mode echocardiography, performed at 8 and 20 weeks, revealed a progressive decline in fractional shortening (FS) and ejection fraction (EF) in 20-week-old dnNRSF Tg mice (Table I and Figure 3F), though FS and EF did not yet differ significantly in 8-week-old mice (Table I). Left ventricular end diastolic dimension (LVDd) and end systolic dimension (LVDs) were also not altered at 8 weeks of age, but by 20 weeks LVDd and LVDs were 30 and 80%, respectively, higher in dnNRSF Tg than NTg mice (Table I). Wall thickness was not significantly affected, indicating progressive LV dysfunction without LV wall hypertrophy in dnNRSF Tg mice.

The results of a hemodynamic analysis using a high-fidelity micromanometer catheter were consistent with the echocardiographic findings and indicated that inhibition of cardiac NRSF is sufficient to cause progressive LV dysfunction (Figure 3G). At 20 weeks of age, dnNRSF Tg mice showed diminished systolic ventricular pressure and significant depression of both the maximal first derivative of the LV pressure (dP/dt_{max}) and the maximal negative derivative of LV pressure (dP/dt_{min}), conditions that were not seen at 8 weeks of age (Table I). Histological examination of cross-sections confirmed LV enlargement without significant increases in wall thickness in 20-week-old dnNRSF Tg hearts (Figure 3H and I). In addition, a marked heterogeneity in the size of ventricular myocytes was noted, with some appearing hypertrophied and others appearing atrophied (Figure 3J–M). No significant inflammatory cell infiltrates were observed in dnNRSF Tg hearts, though Masson's trichrome staining showed the presence of interstitial fibrosis (Figures 3M). Electron microscopic examination of the ultrastructure of ventricular myocytes revealed that, in 20-week-old dnNRSF Tg mice, myofibrils were sparse and misarranged, Z-bands were discontinuous, and mitochondria were deformed or completely disrupted (compare Figure 3N and O with P and Q; arrows indicate disrupted mitochondria). All of these features of dnNRSF Tg mice are characteristic of dilated cardiomyopathy in humans, suggesting that NRSF plays a critical role in the maintenance of normal cardiac structure and function.

Sudden death and ventricular arrhythmias in dnNRSF transgenic mice

Given that dnNRSF Tg mice appeared to die of sudden death, we hypothesized that life-threatening arrhythmias must have occurred. To test this hypothesis, we continuously monitored electrocardiographic data from the mice using implantable radio telemetry. We observed no significant difference in heart rate, QRS time or QT interval between NTg and dnNRSF Tg mice (data not shown). On the other hand, the basal electrocardiograph (ECG) patterns showed the PQ interval to be longer in dnNRSF Tg than NTg mice (dnNRSF Tg, 56.0 ± 3.0 versus NTg, 35.5 ± 0.3 ms; $n = 4$ each, $P < 0.001$). More ominously, second degree AV block (Figure 4A) and ventricular ectopies, including runs of ventricular tachycardia (VT) (Figure 4B and C), were observed in dnNRSF Tg mice. No such rhythm disturbances were observed in NTg mice. During the monitoring period, three dnNRSF Tg mice died suddenly. In each case, VT and ventricular fibrillation (VF) followed by asystole were recorded at the time of death (Figure 4D). Thus, dnNRSF Tg mice exhibit a variety of arrhythmias that are often observed in the human cardiomyopathic heart, culminating in sudden arrhythmic death.

To evaluate further the vulnerability of dnNRSF Tg hearts to ventricular arrhythmias, we performed an

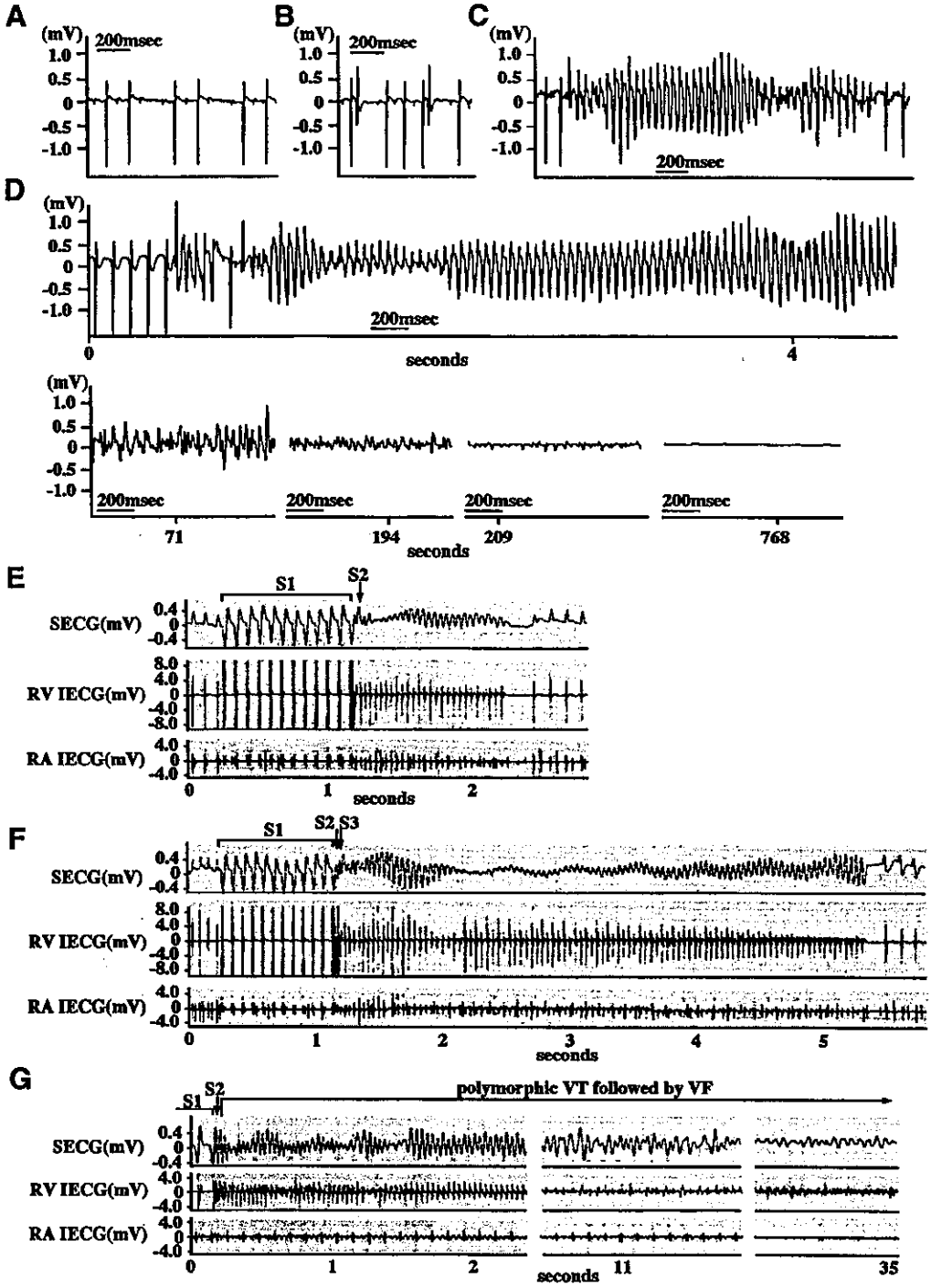

Fig. 4. Spontaneous and inducible arrhythmias in dnNRSF Tg mice. (A–D) ECGs from dnNRSF Tg mice obtained with implantable radio telemetry: second degree AV block (A); isolated ventricular ectopies (B); non-sustained ventricular tachycardia (VT) (C). Sustained VT and ventricular fibrillation (VF) followed by asystole recorded at the time of sudden death (D). (E–G) ECG obtained from dnNRSF Tg mice during electrophysiological studies: polymorphic VT (E and F); sustained polymorphic VT followed by VF (G).

intracardiac electrophysiological analysis using an octapolar EP catheter (Gehrmann and Berul, 1999). To avoid the secondary effects of structural remodeling on the electrophysiological properties, we used 12-week-old dnNRSF Tg and NTg mice whose heart to body weight ratios (Figure 3C) and right ventricular effective refractory periods (dnNRSF Tg, 22.9 ± 1.3 ms versus NTg, 26.0 ± 1.8 ms; n = 6 each) did not differ significantly. When programmed electrical stimulation was applied, VT was induced in six out of 10 dnNRSF Tg mice versus none out of 10 NTg mice (Figures 4E–G). Clearly, dnNRSF Tg hearts were more vulnerable to ventricular arrhythmias than NTg hearts.

Increased expression of fetal-type ion channel genes in dnNRSF transgenic ventricle

The fact that dnNRSF Tg mice exhibit increased vulnerability to arrhythmias and mortality even before develop-

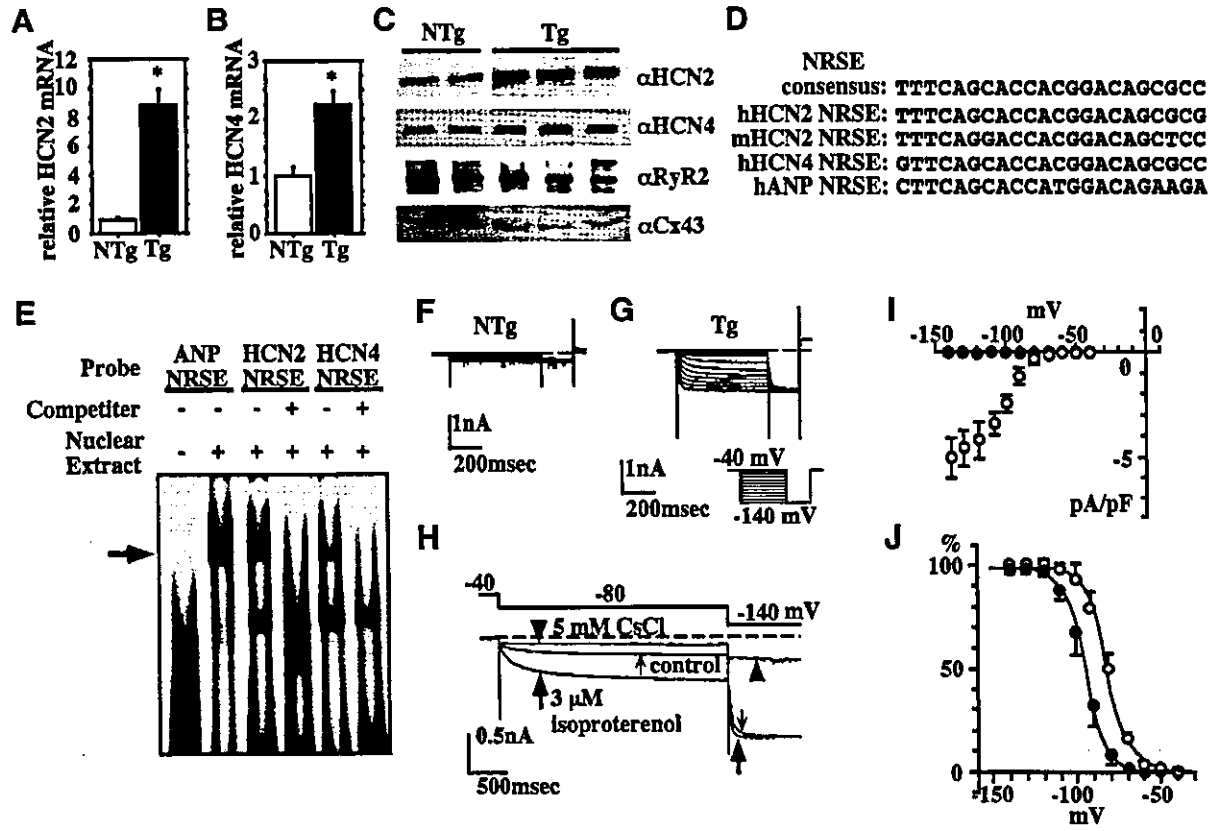

Fig. 5. Increased expression of I_f in dnNRSF Tg hearts. (A and B) Relative levels of *HCN2* (A) and *HCN4* (B) mRNA in the hearts of 8-week-old NTg and dnNRSF Tg mice; $^*P < 0.05$ versus NTg. (C) Western blot analysis of HCN2, HCN4, ryanodine receptor (RYR) 2 and connexin (Cx) 43 in the hearts of 8-week-old NTg and dnNRSF Tg mice. (D) Sequences similar to NRSE in mouse (m) and human (h) *HCN* genes. (E) EMSA was carried out using radiolabeled oligonucleotides from NRSE in *ANP*, *HCN2* or *HCN4* as probes. Unlabeled oligonucleotide from NRSE *ANP* was used as a cold competitor. (F and G) Representative membrane currents elicited by hyperpolarization after complete inhibition of I_{K1} in isolated ventricular myocytes from NTg (F) and dnNRSF Tg (G) mice; the pulse protocol is shown in (G). (H) Pharmacological properties of I_f in ventricular myocytes from dnNRSF Tg mice. Isoproterenol (3 μM) increased the amplitude of I_f during the first conditioning pulse (large arrows), as compared with control (small arrows). The initial current jump at the onset of the second pulse (−140 mV) was concomitantly increased. I_f was completely inhibited by 5 mM Cs^+ (arrow heads). (I) Current–voltage relationship of I_f. The amplitude of the Cs^+-sensitive component was measured at the end of conditioning pulses in ventricular myocytes from NTg (filled circles; $n = 8$) and dnNRSF Tg (open circles; $n = 6$) mice. (J) I_f activation curves measured in the absence (filled circles; $n = 6$) or presence (open circles; $n = 6$) of 3 μM isoproterenol. In (I) and (J), symbols represent means ± SEM.

ment of severe structural abnormalities and cardiac dysfunction suggests that primary alterations in ion channel gene expression are involved. In addition, altered ion channel expression may also participate in the progression of cardiomyopathy in dnNRSF Tg mice. We therefore used murine genome U74A arrays (Affymetrix) to quantify simultaneously expression of ~6000 genes and ~6000 expressed sequence tags (ESTs) in 6-week-old NTg and dnNRSF Tg ventricles, and found that expression of *HCN2/HAC1* is significantly increased in 6-week-old dnNRSF Tg hearts. *HCN2* encodes a channel that carries a hyperpolarization-activated current (I_f) observed in fetal but not normal mature ventricular myocytes, but is reinduced in ventricular myocytes of hypertrophied or failing hearts and may contribute to the increased arrhythmogenicity (Cerbai *et al.*, 1996, 2001). We therefore used quantitative RT–PCR to examine the expression of *HCN2* and *HCN4* mRNA, which are the predominant isoforms expressed in the ventricle (Santoro and Tibbs, 2000). We found that expression of both is significantly upregulated in the hearts of 8-week-old dnNRSF Tg mice (Figure 5A and B). Moreover, western blot analysis confirmed that expression of HCN2 and HCN4 proteins was also upregulated in dnNRSF Tg mice, though ryanodine receptor 2 and connexin 43 were not (Figure 5C). More importantly, sequences highly similar to the 22 bp consensus NRSE (>95% identity) were detected within the first intron of both *HCN2* and *HCN4* (Figure 5D), and electrophoretic mobility shift assays (EMSAs) clearly showed that NRSF binds to NRSE in both genes (Figure 5E). As our previous experiments showed that NRSE can repress multiple promoters in ventricular myocytes (Kuwahara *et al.*, 2001), and others have reported that NRSF represses transcription irrespective of the location or orientation of its binding site within a gene (Thiel *et al.*, 1998), our present findings indicate both *HCN2* and *HCN4* to be downstream targets of NRSF-regulated pathways.

In order to obtain functional evidence of the re-expression of *HCN2* and *HCN4*, we carried out patch-clamp studies using ventricular myocytes isolated from 8- to 14-week-old dnNRSF Tg mice. After the inward-rectifier K^+ current (I_{K1}) was completely inhibited with 0.5 mM Ba^{2+}, no time-dependent current was elicited by hyperpolarization in NTg mice (Figure 5F). In all myocytes from dnNRSF Tg mice, in contrast, hyper-

polarizations more negative than –70 mV activated time-dependent inward currents (Figure 5G). That 5 mM Cs^+ completely blocked these currents confirmed them to be I_f (Figure 5H). The current–voltage relationship of I_f was obtained by subtracting the Cs^+-sensitive component; no Cs^+-sensitive current was recorded in myocytes from NTg mice (Figure 5I). As in pacemaker cells, I_f in ventricular myocytes from dnNRSF Tg mice were augmented by β-adrenergic stimulation (3 μM isoproterenol; Figure 5H) due to a rightward shift in the voltage-dependent activation curve (the potential of half-maximal activation was shifted from –93.3 ± 1.3 to –79.7 ± 1.0 mV; Figure 5J).

The T-type Ca^{2+} current ($I_{Ca,T}$) is also expressed in fetal ventricular myocytes, repressed in mature ventricular myocytes, and reactivated in ventricular myocytes in hypertrophied or failing hearts (Nuss and Houser, 1993; Sen and Smith, 1994; Martinez *et al.*, 1999). Several experiments using a T-type Ca^{2+} channel blocker suggest its involvement in the progression of heart failure (Clozel *et al.*, 1999). Of the two T-type Ca^{2+} channel genes expressed in heart, *CACNA1H* and *CACNA1G*, the former reportedly predominates in fetal ventricle, but is markedly repressed in normal adult heart and reinduced under pathological conditions (Perez-Reyes, 2002; Niwa *et al.*, 2003). Notably, we identified NRSE-like sequences in the first intron of *CACNA1H* (Figure 6A). The NRSE-like sequences in mouse and human *CACNA1H* are 93 and 97%, respectively, identical to the consensus NRSE sequences, and EMSA carried out using NRSE as a probe clearly indicated that NRSF binds to these sequences (Figure 6B). In addition, quantitative RT–PCR showed increased expression of *CACNA1H*, but not *CACNA1G*, in the ventricles of 8-week-old dnNRSF Tg mice (Figure 6C and D). Finally, the Ni^{2+} sensitivity of *CACNA1H*-related currents has been shown to be much higher than that of *CACNA1G*-related currents (Lee *et al.*, 1999). Consistent with that finding, highly Ni^{2+}-sensitive $I_{Ca,T}$ were recorded from ventricular myocytes from dnNRSF Tg mice (Figure 6E) but not NTg mice (Figure 6F), demonstrating the functional expression of *CACNA1H* (Figure 6G). Taken together, these results indicate that NRSF regulates expression of genes encoding the channels that carry the fetal ionic currents I_f and $I_{Ca,T}$.

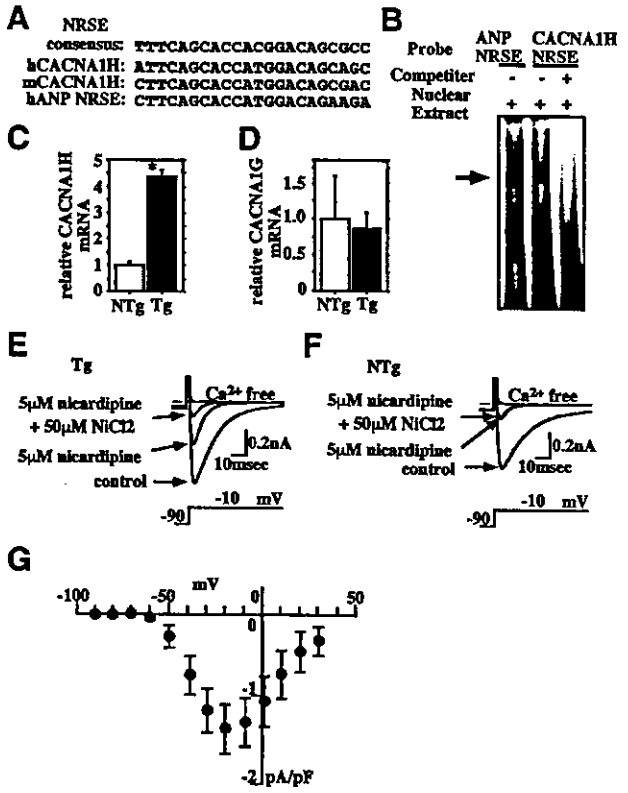

Fig. 6. Increased expression of $I_{Ca,T}$ in dnNRSF Tg hearts. (A) Sequences similar to NRSE in mouse (m) and human (h) *CACNA1H*. (B) EMSA was carried out using a radiolabeled oligonucleotide from NRSE in *ANP* or *CACNA1H* as a probe. Unlabeled oligonucleotide from NRSE in *ANP* was used as a cold competitor. (C and D) Relative levels of *CACNA1H* (C) and *1G* (D) mRNA in the hearts of 8-week-old NTg and dnNRSF Tg mice; $^*P < 0.05$ versus NTg. (E and F) Representative T-type and L-type Ca^{2+} currents in ventricular myocytes from dnNRSF Tg (E) and NTg (F) hearts; the pulse protocol is shown at the bottom. Na^+ current was completely inhibited by 50 μM tetrodotoxin throughout the experiments. Inhibition of the L-type Ca^{2+} current with 5 μM nicardipine revealed the presence of the T-type Ca^{2+} current. (G) The peak I–V relationship of the Ni^{2+}-sensitive T-type Ca^{2+} current measured in the presence of 5 μM nicardipine in ventricular myocytes obtained from dnNRSF Tg mice ($n = 5$). The threshold for the activation was between –60 and –50 mV; symbols represent means ± SEM.

Discussion

NRSF is an important regulator of the fetal cardiac gene program

Reactivation of a fetal gene program is a common feature of cardiac hypertrophy and heart failure; despite much study, however, the mechanism governing such gene reprogramming remains unclear. Our findings that NRSE is selectively present in multiple fetal cardiac genes and that the inhibition of NRSE-mediated repression increases their expression in ventricular myocytes, both *in vitro* and *in vivo*, are indicative of the significance of the NRSE–NRSF system to the regulation of the fetal cardiac gene program. Indeed, we showed there to be a reciprocal relationship between the levels of *NRSF* and *ANP* mRNA expression in fetal and adult ventricles, which strongly suggests that NRSF represses fetal cardiac gene expression in terminally differentiated ventricular myocytes. We also demonstrated that inhibition of NRSF diminishes the capacity of hypertrophic stimuli to increase the transcriptional efficiency of fetal cardiac genes. Conversely, the presence of full-length NRSF significantly reduces the basal *ANP* promoter activity and increases the responsiveness of its activity to ET-1. Thus, NRSF appears to be involved not only in the repression of basal expression of fetal cardiac genes but also in the reinduction of fetal cardiac gene expression during cardiac hypertrophy. That ventricular *NRSF* expression is diminished in a mouse model of load-induced cardiac hypertrophy, in sharp contrast to *BNP* expression, is consistent with that view.

NRSF contributes to the maintenance of normal cardiac structure and function

The present findings suggesting a decrease in NRSF repressor activity to be a component of the hypertrophic signal leading to the upregulation of fetal gene expression prompted us to examine the consequences of persistent inhibition of NRSF on the function of post-natal hearts. It

is notable that heart-specific inactivation of NRSF was sufficient to cause dilated cardiomyopathy, which suggests that NRSF plays a critical role in the structural and functional alterations that occur during the development of heart failure. It is not completely clear at present which of the primary genetic alterations induced by NRSF inhibition initiate the subsequent remodeling process that leads to dilated cardiomyopathy, though there is a possibility that constitutive expression of *α-skeletal actin* in adult heart contributes to the progression to LV dysfunction. In normal, mature ventricular myocytes, cardiac α-actin comprises ~80% of the total actin protein, with α-skeletal actin comprising the remaining 20%. Induction of *α-skeletal actin* expression in dnNRSF Tg hearts could change the normal ratio of the two actin isoforms, thereby impairing cardiac function; indeed, actin dysfunction is known to lead to heart failure (Olson *et al.*, 1998). Also, the fact that constitutive expression of β-MHC, another fetal cardiac isoform of a contractile protein, is sufficient to reduce systolic function further supports this view (Tardiff *et al.*, 2000). It is unlikely that increased production of ANP and BNP causes the dilated cardiomyopathy and sudden death seen in dnNRSF Tg mice: *BNP* transgenic mice exhibit no pathological phenotypes in the heart, though *BNP* knockout mice do show interstitial fibrosis (Ogawa *et al.*, 1994; Tamura *et al.*, 2000). In addition, dnNRSF Tg mice lacking the guanylyl cyclase-A gene, encoding the receptor for ANP and BNP, still showed increased mortality and severe cardiomyopathic phenotype (unpublished observation).

We recently found that the class II HDACs, HDAC4 and 5, which reportedly act as signal-responsive repressors in molecular pathways governing cardiac hypertrophy and heart failure (Zhang *et al.*, 2002), associate with NRSF and modulate its repressor function in ventricular myocytes (unpublished observation). Thus further investigation will be required before complete characterization of the mechanisms involved in the development of dilated cardiomyopathy, the modulation of NRSF function, and the role of NRSF in pathogenesis of heart failure is achieved.

Our results also demonstrate that NRSF regulates ventricular expression of genes encoding fetal-type ion channels carrying I_f and $I_{Ca,T}$. In adult hearts, expression of I_f and $I_{Ca,T}$ is restricted to pacemaker cells and his-Purkinje fibers. Although it is still controversial, I_f and $I_{Ca,T}$ appear to participate in automaticity of the pacemaker cells (Santoro and Tibbs, 2000; Shorofsky and Balke, 2001). Re-expression of these channels in the hypertrophied or failing ventricle may therefore increase the automaticity of ventricular myocytes, giving rise to arrhythmias. Alternatively, the arrhythmogenesis in dnNRSF Tg mice may be due to Ca^{2+} overload and delayed after-depolarization of ventricular myocytes. The channel carrying I_f is highly permeable to both Na^+ and K^+, and continuous activation of I_f at the resting membrane potential, particularly during adrenergic stimulation, may cause Na^+ to accumulate within myocytes. The resultant decrease of driving force for the Na^+–Ca^{2+} exchanger could in turn lead to Ca^{2+} overload. Likewise, overexpression of $I_{Ca,T}$ could also contribute to Ca^{2+} overload, thereby leading to arrhythmogenesis.

In similar fashion, alterations in I_f and $I_{Ca,T}$ may contribute to the development of cardiac dysfunction in dnNRSF Tg mice. Recent reports indicate that intracellular Na^+ is elevated in hypertrophied and failing hearts, and that the increased intracellular Na^+ may play an important role for the initiation and progression of heart failure (Pieske and Houser, 2003; Pogwizd *et al.*, 2003). An increase in Na^+ influx carried by I_f can directly affect intracellular Ca^{2+} handling via the Na^+–Ca^{2+} exchanger and lead to cardiac dysfunction, while increased $I_{Ca,T}$ expression reportedly increases diastolic intracellular Ca^{2+}, profoundly affecting cardiac function (Clozel *et al.*, 1999). Taken together, these findings suggest that dysregulation of the expression of the fetal ionic channels carrying I_f and $I_{Ca,T}$ may contribute, at least in part, to the progression of dilated cardiomyopathy, as well as to the increased vulnerability to arrhythmias in dnNRSF Tg mice.

In summary, we have shown NRSF to be a crucial transcriptional regulator contributing to the maintenance of the normal mature phenotype of cardiac myocytes by repressing expression of several fetal cardiac genes, including those encoding natriuretic peptides (*ANP* and *BNP*), a fetal isoform of a contractile protein (*α-skeletal actin*) and fetal ion channels (*HCN2*, *HCN4* and *CACNA1H*). NRSF is also involved in the reactivation of the fetal gene program during cardiac muscle cell hypertrophy, and persistent inhibition of NRSF function causes dilated cardiomyopathy and leads to the increased vulnerability to arrhythmias and sudden death. NRSF thus appears to play a key role in the progression of cardiac dysfunction and lethal arrhythmias associated with heart failure. Normalization of dysregulated cardiac gene expression through restoration or enhancement of NRSF repressor function may represent a new therapeutic strategy for preventing the progression of heart failure and sudden death.

Materials and methods

Plasmid constructs

Five GAL4-binding sites were inserted upstream of the *ANP* promoter (–452 to +97), which had been inserted into the *BglII–HindIII* sites of PGV-B2 (TOYO INK Inc., Tokyo, Japan), yielding a plasmid designated 5UAS-ANPLuc. Plasmids encoding mouse full-length NRSF and dnNRSF were kindly provided by D.J.Anderson. A plasmid encoding GAL4-NRSF was constructed within the pBIND vector (Promega, Madison, WI) as previously described (Kuwahara *et al.*, 2001).

Ventricular myocyte culture and transfection

Preparation, transfection, adenoviral infection and culture of rat neonatal ventricular myocytes were carried out as previously described (Kuwahara *et al.*, 2001).

Generation of α-MHC-dnNRSF transgenic mice

A dnNRSF cDNA (along with a 5′ myc epitope tag) was cloned into the *SalI–HindIII* site of a pBluescript II KS (+) plasmid containing the *α-MHC* promoter (a generous gift from J.Robbins). The *α-MHC-dnNRSF* transgenic construct was then released from the vector backbone by digestion with *NotI* and purified for injection into the pronucleus of fertilized oocytes derived from C57BL/6J mice, after which the surviving embryos were transferred to the oviducts of pseudopregnant MCH(ICR) mice. Transgenic founders were identified by either Southern blot analysis or PCR. dnNRSF expression was confirmed by western blot analysis using anti-myc tag antibody (Santa Cruz Biotechnology, Inc., Santa Cruz, CA). Determination of expression levels of the *dnNRSF* gene is described in the Supplementary data available at *The EMBO Journal*

Online. Pressure overload was produced by TAC as described previously (Harada *et al.*, 1998). The care of the animals and all experiments were conducted in accordance with the institutional guidelines of Kyoto University Graduate School of Medicine.

Intracardiac electrophysiology

Mice were intubated and anesthetized with 0.5–1.5% isoflurane, and surface ECGs (limb leads) were placed. With a 1.7 French octapolar catheter (CIBer mouse EP, NuMe, Hopkinton, NY) inserted via a jugular vein, the standard EPS protocol was performed as described previously (Gehrmann and Berul, 1999). Rapid ventricular pacing using the extrastimulation (S_1S_2) technique was performed with 1–2 extra stimuli to determine the ventricular refractory period and to attempt induction of ventricular arrhythmias. The stimulation was performed at twice the ventricular diastolic capture threshold.

Analysis of electrocardiographs by telemetry

To monitor ambulatory ECGs, radio frequency transmitters (TA 10ETA-F20; Data Science, St Paul, MN) were implanted as previously described (Lee *et al.*, 1998).

Electrophysiological recording from isolated ventricular myocytes

Myocytes were isolated from the left ventricle as previously described (Powell *et al.*, 1980). Whole-cell patch–clamp was then carried out using K^+-rich pipet solution containing 145 mM KCl, 5.0 mM MgATP, 5 mM Na_2 creatine phosphate, 5 mM EGTA, 0.1 mM Na_2GTP, 5 mM HEPES 5 (pH 7.2 with KOH) and physiological bathing solution (phosphate-buffered saline; PBS) containing 140 mM NaCl, 5.4 mM KCl; 0.5 mM $MgCl_2$, 1.8 mM $CaCl_2$, 5 mM HEPES and 5 mM glucose (pH 7.4 with NaOH). I_f was recorded in PBS containing 0.5 mM $BaCl_2$. Alternatively, when recording $I_{Ca,T}$, the pipet solution contained: 100 mM CsCl, 50 mM *N*-methyl-D-glutamine, 10 mM tetraethyl ammonium chloride (TEA), 5 mM MgATP, 10 mM BAPTA and 5 mM HEPES (pH 7.2 with HCl). After formation of the giga-seal in PBS, the myocytes were superfused with TEA–Cs bathing solution containing 100 mM NaCl, 40 mM TEA, 5.4 mM CsCl, 0.5 mM $MgCl_2$, 1.8 mM $CaCl_2$, 5 mM HEPES, 5 mM glucose and 0.05 mM tetrodotoxin (pH 7.4 with NaOH). All recordings were made at 32–34°C.

Statistical analysis

Data are presented as means ± SEM. Unpaired *t*-test was used for comparison between two groups, and ANOVA with *post hoc* Fisher's tests was used for comparison among groups. Values of $P < 0.05$ were considered significant. An inverse correlation between cardiac BNP and NRSF mRNA levels was examined by linear regression analysis.

Supplementary data

Supplementary data are available at *The EMBO Journal* Online.

Acknowledgements

We thank Ms Okamura for her secretarial work. This work was supported in part by research grants from the Japanese Ministry of Education, Science and Culture, the Japanese Ministry of Health and Welfare, the Japanese Society for the Promotion of Science 'Research for the Future' program (JSPS-RFTF96I00204 and JSPS-RFTF98L00801), JSPS Research Fellowships for Young Scientists, Japanese Heart Foundation Research Grant, Japanese Heart Foundation/Pfizer Pharmaceuticals Inc. Grant on Cardiovascular Disease Research, Kanae Foundation for Life and Socio-Medical Science, the Mochida Memorial Foundation for Medical and Pharmaceutical Research, the Promotion of Fundamental Studies in Health Science of the Organization for Pharmaceutical Safety and Research (OPSR) of Japan, and the Takeda Science Foundation.

References

Cerbai,E., Barbieri,M. and Mugelli,A. (1996) Occurrence and properties of the hyperpolarization-activated current I_f in ventricular myocytes from normotensive and hypertensive rats during aging. *Circulation*, **94**, 1674–1681.

Cerbai,E. *et al.* (2001) The properties of the pacemaker current I_f in human ventricular myocytes are modulated by cardiac disease. *J. Mol. Cell. Cardiol.*, **33**, 441–448.

Chen,Z.F., Paquette. A.J. and Anderson,D.J. (1998) NRSF/REST is required *in vivo* for repression of multiple neuronal target genes during embryogenesis. *Nature Genet.*, **20**, 136–142.

Chien,K.R., Knowlton,K.U., Zhu,H. and Chien,S. (1991) Regulation of cardiac gene expression during myocardial growth and hypertrophy: molecular studies of an adaptive physiologic response. *FASEB J.*, **5**, 3037–3046.

Chong,J.A. *et al.* (1995) REST: a mammalian silencer protein that restricts sodium channel gene expression to neurons. *Cell*, **80**, 949–957.

Clozel,J.P., Ertel,E.A. and Ertel,S.I. (1999) Voltage-gated T-type Ca^{2+} channels and heart failure. *Proc. Assoc. Am. Physicians*, **111**, 429–437.

Gehrmann,J. and Berul,C.I. (1999) Cardiac electrophysiology in genetically engineered mice. *J. Cardiovasc. Electrophysiol.*, **11**, 354–368.

Grimes,J.A. *et al.* (2000) The co-repressor mSin3A is a functional component of the REST–CoREST repressor complex. *J. Biol. Chem.*, **275**, 9461–9467.

Harada,K., Komuro,I., Zou,Y., Kudoh,S., Kijima,K., Matsubara,H., Sugaya,T., Murakami,K. and Yazaki,Y. (1998) Acute pressure overload could induce hypertrophic response in the heart of angiotensin II type1a knockout mice. *Circ. Res.*, **82**, 779–785.

Kjær,A. and Hesse,B. (2001) Heart failure and neuroendocrine activation: diagnostic, prognostic and therapeutic perspectives. *Clin. Physiol.*, **21**, 661–672.

Kraner,S.D., Chong,J.A., Tsay,H.J. and Mandel,G. (1992) Silencing the type II sodium channel gene: a model for neural-specific gene regulation. *Neuron*, **9**, 37–44.

Kuwahara,K. *et al.* (2001) The neuron-restrictive silencer element–neuron-restrictive silencer factor system regulates basal and endothelin 1-inducible atrial natriuretic peptide gene expression in ventricular myocytes. *Mol. Cell. Biol.*, **21**, 2085–2097.

Lee,J.H., Gomora,J.C., Cribbs,L.L. and Perez-Reyes,E. (1999) Nickel block of three cloned T-type calcium channels: low concentrations selectively block α1H. *Biophys. J.*, **77**, 3034–3042.

Lee,P. *et al.* (1998) Conditional lineage ablation to model human diseases. *Proc. Natl Acad. Sci. USA*, **95**, 11371–11376.

Martinez,M.L., Heredia M.P. and Delgado,C. (1999) Expression of T-type Ca^{2+} channels in ventricular cells from hypertrophied rat hearts. *J. Mol. Cell. Cardiol.*, **31**, 1617–1625.

Mori,N., Schoenherr,C.J., Vandenbergh,D.J. and Anderson,D.J. (1992) A common silencer element in the SCG10 and type II Na^+ channel genes binds a factor present in nonneuronal cells but not in neuronal cells. *Neuron*, **9**, 45–54.

Niwa,N., Hojo,M., Takemura,H., Horiba,M., Lee,J., Yasui,K. and Kodama,I. (2003) Recapturation of early embryonic T-type Ca^{2+} channel genes (α1h) in mouse remodeled hearts after myocardial infarction. *Circ. J.*, **67**, 503.

Nuss,H.B. and Houser,S.R. (1993) T-type Ca^{2+} current is expressed in hypertrophied adult feline left ventricular myocytes. *Circ. Res.*, **73**, 777–782.

Ogawa,E. *et al.* (2002) Fibronectin stimulates BNP gene transcription by inhibiting neuron-restrictive silencer element-dependent repression. *Cardiovasc. Res.*, **53**, 451–459.

Ogawa,Y. *et al.* (1994) Molecular cloning of the complementary DNA and gene that encode mouse brain natriuretic peptide and generation of transgenic mice that overexpress the brain natriuretic peptide gene. *J. Clin. Invest.*, **93**, 1911–1921.

Olson,T.M., Michels,V.V., Thibodeau,S.N., Tai,Y.S. and Keating,M.T. (1998) Actin mutation in dilated cardiomyopathy, a heritable form of heart failure. *Science*, **280**, 750–752.

Palm,K., Belluardo,N., Metsis,M. and Timmusk,T. (1998) Neuronal expression of zinc finger transcription factor REST/NRSF/XBR gene. *J. Neurosci.*, **18**, 1280–96.

Perez-Reyes,E. (2002) Molecular physiology of low-voltage-activated T-type calcium channels. *Physiol. Rev.*, **83**, 117–161.

Pieske,B. and Houser,S.R. (2003) $[Na^+]_I$ handling in the failing human heart. *Cardiovasc. Res.*, **57**, 874–886.

Pogwizd,S.M., Sipido,K.R., Verdonck,F. and Bers,D.M. (2003) Intracellular Na in animal model of hypertrophy and heart failure: contractile function and arrhythmogenesis. *Cardiovasc. Res.*, **57**, 887–896.

Powell,T., Terrar,D.A. and Twist,V.W. (1980) Electrophysiological properties of individual cells isolated from adult rat ventricular myocardium. *J. Physiol.*, **302**, 131–153.

Santoro,B. and Tibbs,G. (2000) The HCN gene family: molecular basis

of the hyperpolarization-activated pacemaker channels. *Ann. NY Acad. Sci.*, **868**, 741–764.
Schoenherr,C.J. and Anderson,D.J. (1995) The neuron-restrictive silencer factor (NRSF): a coordinate repressor of multiple neuron-specific genes. *Science*, **267**, 1360–1363.
Schoenherr,C.J., Paquette,A.J. and Anderson,D.J. (1996) Identification of potential target genes for the neuron-restrictive silencer factor. *Proc. Natl Acad. Sci. USA*, **93**, 9881–9886.
Sen,L. and Smith,T.W. (1994) T-type Ca^{2+} channels are abnormal in genetically determined cardiomyopathic hamster hearts. *Circ. Res.*, **75**, 149–155.
Shorofsky,S.R. and Balke,W. (2001) Calcium currents and arrhythmias: insights from molecular biology. *Am. J. Med.*, **110**, 127–140.
Subramaniam,A., Jones,W.K., Gulick,J., Wert,S., Neumann,J. and Robbins,J. (1991) Tissue-specific regulation of the α-myosin heavy chain gene promoter in transgenic mice. *J. Biol. Chem.*, **266**, 24613–24620.
Tamura,N. *et al.* (2000) Cardiac fibrosis in mice lacking brain natriuretic peptide. *Proc. Natl Acad. Sci. USA*, **97**, 4239–4244.
Tardiff,J.C., Hewett,T.E., Factor,S.M., Vilkstrom,K.L., Robbins,J. and Leinwand,L.A. (2000) Expression of the β (slow)-isoform of MHC in the adult mouse heart causes dominant-negative functional effects. *Am. J. Physiol.*, **278**, H412–H419.
Thiel,G., Lietz,M. and Cramer,M. (1998) Biological activity and modular structure of RE-1 silencing transcription factor (REST), a repressor of neuronal genes. *J. Biol. Chem.*, **273**, 26891–26899.
Tomaselli,G.F. and Marbán,E. (1999) Electrophysiological remodeling in hypertrophy and heart failure. *Cardiovasc. Res.*, **42**, 270–283.
Zhang,C.L., McKinsey,T.A., Chang,S., Antos,C.L., Hill,J.A. and Olson,E.N. (2002) Class II histone deacetylases act as signal-responsive repressors of cardiac hypertrophy. *Cell*, **110**, 479–488.

Received June 20, 2003; revised September 12, 2003; accepted October 13, 2003

FEBS Letters 544 (2003) 86–92 FEBS 27287

Adrenomedullin provokes endothelial Akt activation and promotes vascular regeneration both in vitro and in vivo

Kazutoshi Miyashita, Hiroshi Itoh*, Naoki Sawada, Yasutomo Fukunaga, Masakatsu Sone, Kenichi Yamahara, Takami Yurugi-Kobayashi, Kwijun Park, Kazuwa Nakao

Department of Medicine and Clinical Science, Kyoto University Graduate School of Medicine, 54 Shogoin Kawahara-cho Sakyo-ku, Kyoto 606-8507, Japan

Received 18 February 2003; revised 14 April 2003; accepted 15 April 2003

First published online 14 May 2003

Edited by Beat Imhof

Abstract **We previously reported that adrenomedullin (AM), a vasodilating hormone secreted from blood vessels, promotes proliferation and migration of human umbilical vein endothelial cells (HUVECs). In this study, we examined the ability of AM to promote vascular regeneration. AM increased the phosphorylation of Akt in HUVECs and the effect was inhibited by the AM antagonists and the inhibitors for protein kinase A (PKA) or phosphatidylinositol 3-kinase (PI3K). AM promoted re-endothelialization in vitro of wounded monolayer of HUVECs and neo-vascularization in vivo in murine gel plugs. These effects were also inhibited by the AM antagonists and the inhibitors for PKA or PI3K. The findings suggest that AM plays significant roles in vascular regeneration, associated with PKA- and PI3K-dependent activation of Akt in endothelial cells, and possesses therapeutic potential for vascular injury and tissue ischemia.**

Key words: Adrenomedullin; cAMP; Akt; Angiogenesis; Re-endothelialization; Vascular regeneration

1. Introduction

Vascular regeneration is an essential event in recovery from endothelial injury or tissue ischemia. Thus, therapeutic strategies to promote re-endothelialization or neo-vascularization are now highlighted as promising treatment for atherosclerotic or ischemic diseases [1,2]. Many vasoactive substances secreted from endothelial cells (vascular hormones) have been reported to regulate not only vascular tone but also remodeling or regeneration. We revealed that C-type natriuretic peptide (CNP) is secreted from endothelial cells [3] and gene transfer of CNP promoted endothelial regeneration [4,5] and ischemia-induced angiogenesis [6] in vivo. We also reported that NPs directly promote endothelial regeneration in vitro [7]. In this way, NPs/cGMP/cGMP-dependent kinase (cGK) cascade is elucidated to be involved in the regulation of vascular regeneration.

Adrenomedullin (AM) is a potent vasorelaxant peptide that was originally isolated from human pheochromocytoma cells on the basis of its effect to elevate cAMP levels in rat platelets [8,9]. Recently, mice genetically engineered to overexpress or underexpress the AM gene were developed to determine the in vivo significance of AM [10–12]. Mice overexpressing the AM gene in their vasculature showed reduced blood pressure. On the other hand, mice lacking the AM gene did not survive the embryonic stage and showed abnormal vascular structure and subcutaneous hemorrhage. These observations suggest the significance of AM in vascular morphogenesis and regulation of vascular tone in vivo. AM has been shown to be present in atherosclerotic lesions and its secretion has been demonstrated to be augmented by inflammatory cytokines such as interleukin-1, TNF-α, and lipopolysaccharide [13]. Furthermore, hypoxia-responsive elements were identified in the AM gene and hypoxic conditions were reported to induce its expression and secretion from HUVECs [14]. These findings suggest the significance of AM for atherogenesis and angiogenesis.

Based on these findings, together with our recent report to show that AM enhanced proliferation and migration of cultured endothelial cells [15], we hypothesized that AM/cAMP/protein kinase A (PKA) cascade might have the potency to promote vascular regeneration. In this study, we tried to clarify whether AM has beneficial effects on vascular regeneration in the physiological in vitro model for endothelial regeneration and in vivo neo-vascularization in murine gel plugs.

2. Materials and methods

2.1. Materials and cell culture

All agents used were commercially available. Human AM, rat AM, proadrenomedullin N-terminal 20 peptide (PAMP), and the two AM antagonists, AM(22–52) and calcitonin gene-related peptide (8–37) (CGRP(8–37)) were purchased from the Peptide Institute (Osaka, Japan). The two PKA inhibitors, adenosine 3′,5′-cyclic monophosphorothioate Rp-isomer (Rp-cAMP) and myristoylated PKA inhibitor peptide sequence (14–22) cell-permeable (PKA Inh. Peptide), the two phosphatidylinositol 3-kinase (PI3K) inhibitors, LY294002 and wortmannin, and a cAMP analog, 8-Br-cAMP, were purchased from Calbiochem (San Diego, CA, USA). Vascular endothelial growth factor (VEGF) was purchased from Peprotech (London, UK).

HUVECs (Clonetics, Waltersville, MD, USA) were grown in the basic medium containing 2% fetal bovine serum (FBS) and growth supplements (EGM-2; Clonetics). Cell cultures between passages 4 and 6 were used for each experiment.

*Corresponding author. Fax: (81)-75-771 9452.
E-mail address: hiito@kuhp.kyoto-u.ac.jp (H. Itoh).

Abbreviations: AM, adrenomedullin; PKA, protein kinase A; PI3K, phosphatidylinositol 3-kinase; HUVEC, human umbilical vein endothelial cell; NP, natriuretic peptide; PKA Inh. Peptide, myristoylated protein kinase A inhibitor peptide sequence (14–22) cell-permeable; FBS, fetal bovine serum

0014-5793/03/$22.00
doi:10.1016/S0014-5793(03)00484-8

2.2. Western blot analysis of phosphorylated Akt

HUVECs were treated with or without AM (10^{-8} mol/l) and they were harvested 30 min after the treatments otherwise indicated. Western blotting was performed according to a standard protocol, as we described previously [16]. Akt activity was evaluated by the ratio of phosphorylated Akt to total Akt detected by phospho-Akt (Ser473) and Akt antibody (Cell Signaling, Beverly, MA, USA), respectively. To evaluate Akt activation in endothelial injury, artificial wounds were made by a blue-tip at intervals of 5 mm on an over-confluent monolayer of HUVECs. Densitometric assays were done and the results were presented as fold increase compared to the control.

2.3. Wound healing assay in vitro

To examine whether AM promotes endothelial regeneration in vitro, wound healing assay was carried out as we described previously [7]. In the report, we confirmed that this assay could evaluate overall activity of endothelial proliferation and migration. Briefly, HUVECs were grown to over-confluent in six-well plates and a wound of approximately 2 mm width was made by a cell scraper. Cells were allowed to repair the wound for 40 h in the medium containing 0.5% FBS with or without experimental agents. The wounded monolayer was photographed before and after the incubation period and the re-endothelialized area was evaluated.

2.4. Gel plug assay in vivo

To examine the ability of AM to induce neo-vascularization in vivo, we used murine MATRIGEL plug assay, as described previously [17]. Mice were handled with care according to accepted ethical guidelines. Nude mice were anesthetized with pentobarbiturate (80 mg/kg) and 400 μl per plug of growth factor-reduced phenol red-free MATRIGEL (Becton Dickinson, Bedford, MA, USA) was injected into the abdomen of 6–8 week old male KSN-nude mice (Japan SLC; Hamamatsu, Japan) subcutaneously. A mouse was injected two gels symmetrically in the abdomen, gels with and without experimental agents.

On day 0, 4, 7, 14, and 21, the margins of the subcutaneous plugs were marked and the mean blood flow and the size of the plugs were estimated by a laser Doppler perfusion image analyzer (Moor instruments, Devon, UK). Blood flow in the plug was calculated by the formula: (blood flow) = (mean blood flow) × (plug size). The ratio of the blood flow of the two plugs in the same mouse, an agent-containing plug to its control plug, was considered to be the index of the angiogenic activity of the agent.

The gel plugs were resected from mice on day 21 and stained with rat anti-mouse PECAM-1 (Pharmingen, San Diego, CA, USA) and the number of PECAM-1 positive cells in the plug was estimated as capillary density. 1-mm thick slices were also processed and stained with rat anti-mouse PECAM-1 and a fluorescent agent, Alexa Flour 488 conjugated goat anti-rat IgG (Molecular Probes, Eugene, OR, USA) for the observation with a confocal microscope (LSM5 PASCAL; Carl Zeiss, Oberkochen, Germany) that can reconstruct the 3D structure of the plug from the obtained consecutive images. In this way, small capillaries in the plug were visualized stereoscopically.

2.5. Statistics

All data are expressed as the mean ± S.E.M. Statistical analysis was performed with ANOVA (analysis of variance) or Student's *t*-test. Values of $P < 0.05$ were considered to be statistically significant.

3. Results

3.1. AM activated Akt in HUVECs in a PKA- and PI3K-dependent manner

Fig. 1A demonstrates a time course of the phosphorylation of Akt at amino acid residue 473 (serine) after the treatment with AM (10^{-8} mol/l) on HUVECs. Akt phosphorylation was augmented within 15 min and peaked at 30 min.

To examine Akt activation in endothelial damage, we made artificial wounds in a confluent monolayer of HUVECs as described in Section 2. The endothelial injury itself increased Akt phosphorylation and the addition of AM to the injured endothelium further augmented the increase (Fig. 1B).

AM-induced phosphorylation of Akt was inhibited by the two AM antagonists, AM(22–52) (10^{-5} mol/l) and CGRP-(8–37) (10^{-5} mol/l). The PKA inhibitors, Rp-cAMP (10^{-5} mol/l) and PKA Inh. Peptide (5×10^{-7} mol/l), and the inhibitors for PI3K, LY294002 (10^{-5} mol/l) and wortmannin (10^{-7} mol/l), also suppressed Akt phosphorylation significantly (Fig. 1C).

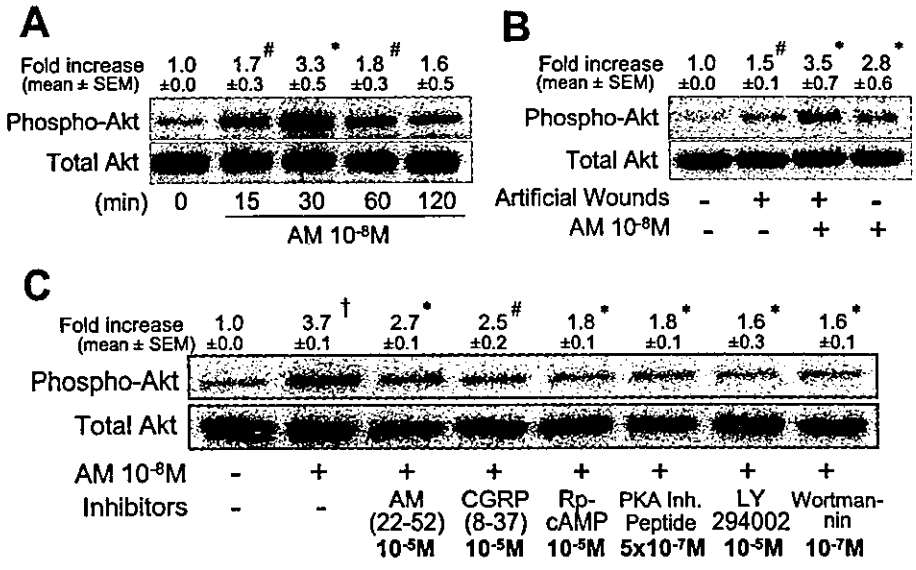

Fig. 1. Effect of AM on Akt activation in HUVECs. A: Time course of Akt phosphorylation in AM-treated HUVECs. Cells were treated with AM (10^{-8} mol/l) and harvested at the indicated times. B: Effect of artificial wounds and AM on Akt phosphorylation. Wounds were made at intervals of 5 mm on an over-confluent monolayer of HUVECs treated with or without AM. Cells were harvested 30 min after the treatments and phosphorylated Akt was detected. C: Effect of the AM antagonists and the inhibitors for PKA or PI3K on AM-induced Akt phosphorylation in HUVECs. Cells were pre-incubated with these inhibitors for 15 min before the administration of AM. They were harvested 30 min after the treatment and phosphorylated Akt was detected. Densitometric analyses were done and the ratio of phosphorylated Akt to total Akt is presented as fold increases compared to the control. #: $P<0.05$; *: $P<0.01$ versus the control (panels A and B) or the AM-treated group without inhibitors (panel C); †: $P<0.01$ versus the control (panel C), $n=3$.

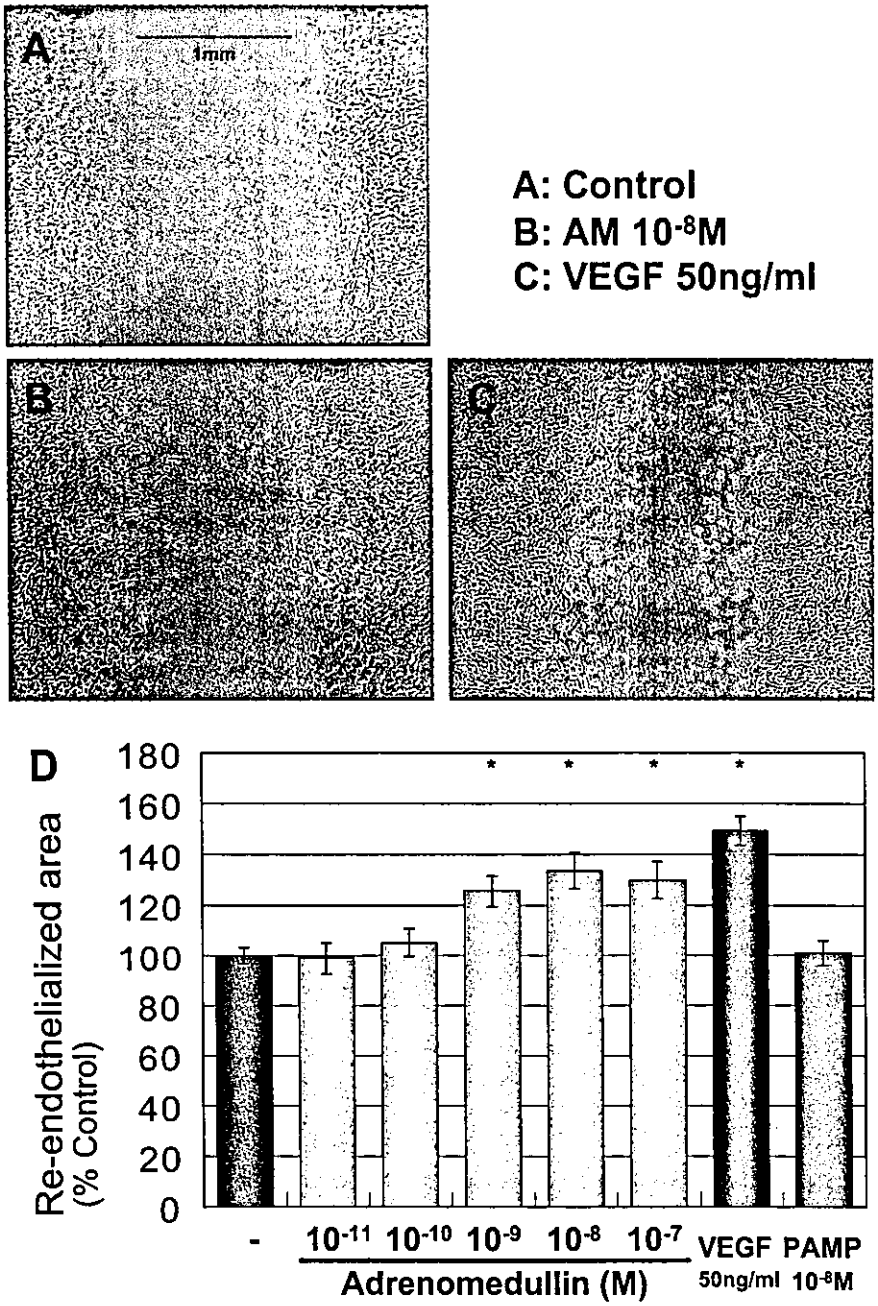

Fig. 2. Effect of AM on endothelial regeneration in wound healing assay in vitro. Wounded monolayer of HUVECs was incubated for 40 h. A–C: Representative photographs of re-endothelialized monolayer incubated for 40 h with the medium containing 0.5% FBS (control) (panel A), accompanied by AM (panel B), or VEGF (panel C). D: Dose-dependent effect of AM on endothelial regeneration in comparison to VEGF and PAMP. *: $P < 0.01$ versus the control, $n = 12$.

3.2. *AM promoted re-endothelialization of the wounded monolayer of HUVECs through a PKA- and PI3K-dependent pathway*

Fig. 2 shows the closure of wounded endothelium incubated with FBS 0.5% (control) (Fig. 2A), accompanied with AM (10^{-8} mol/l) (Fig. 2B), or VEGF (50 ng/ml) (Fig. 2C) for 40 h. Accelerated wound closure was observed in the group treated with AM, as well as that treated with VEGF. Fig. 2D shows the dose-dependent effect of AM on endothelial regeneration in comparison with VEGF and PAMP. AM promoted the wound closure significantly and dose-dependently. The increase of re-endothelialized area by 10^{-8} mol/l AM was 33.6% ± 7.1% over the control ($P < 0.01$, $n = 12$). On the other hand, PAMP, a hypotensive peptide that is synthesized from the same precursor of AM, had no significant effect on endothelial regeneration.

We next examined the effect of the same inhibitors at the same concentrations which were used in Akt phosphorylation assay and had a significant inhibitory effect on AM-induced Akt activation. The two AM antagonists and the inhibitors for PKA or PI3K at those concentrations suppressed AM (10^{-8} mol/l)-induced endothelial regeneration without affecting basal wound closure (Table 1).

In addition, 8-Br-cAMP (10^{-9} mol/l) mimicked the AM action to promote endothelial regeneration in wound healing assay (21.8% ± 5.0% over the control, $P < 0.01$, $n = 8$).

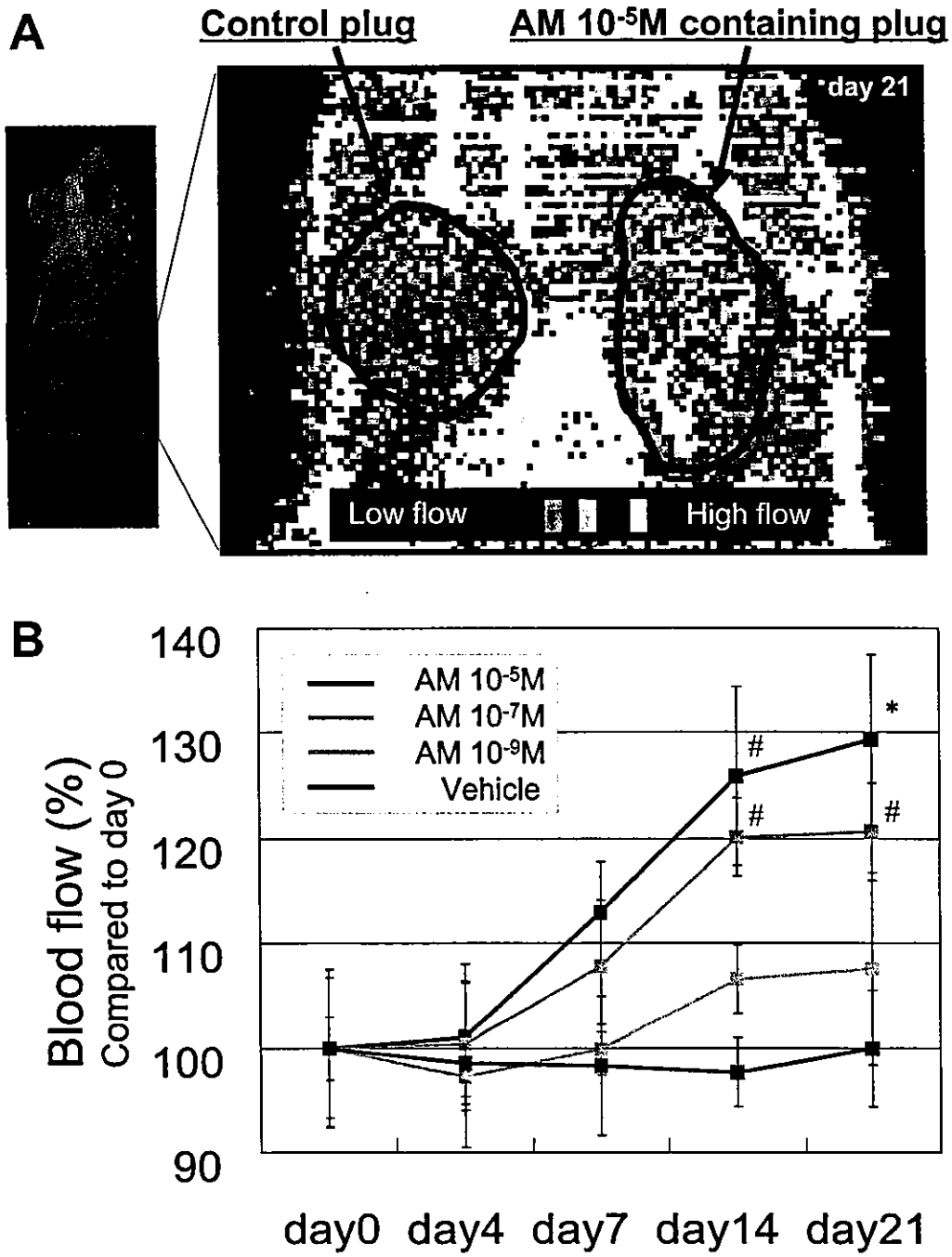

Fig. 3. Effect of AM on blood perfusion in murine gel plug assay. A: Blood flow measurement by a laser Doppler perfusion image analyzer. A representative view of a mouse injected with an AM-containing gel (10^{-5} mol/l) and a control gel is shown. The high-flow area is depicted in red to white and the low-flow in green to black. B: Time course of the effect of AM on blood flow in gel plugs. Blood flow on each day was measured by the laser Doppler perfusion image analyzer and compared to that on day 0. #: $P<0.05$; *: $P<0.01$ versus the blood flow on day 0. $n=12$ (AM 10^{-5} mol/l group), 8 (AM 10^{-7} mol/l and vehicle groups), and 4 (AM 10^{-9} mol/l group).

3.3. *AM augmented blood flow in the plug through a PKA- and PI3K-dependent pathway*

Fig. 3A demonstrates a representative image of the blood flow analysis of gel plugs on day 21. The AM-containing plug presented significantly higher blood perfusion compared to its control plug. The blood flow of the 10^{-5} mol/l AM-containing plug on day 21 was 29.4% ± 8.1% higher than that on day 0 ($P<0.01$, $n=12$; Fig. 3B).

The effects of the inhibitors on the AM-induced increase in blood flow were examined. Inclusion of the AM antagonists and the inhibitors for PKA or PI3K in AM-containing plugs significantly suppressed AM (10^{-7} mol/l)-induced augmentation of blood flow (Table 2).

The inhibitors at the doses used in the MATRIGEL plug assay had no significant effect on basal blood flow (Table 2) and the number of neo-vessels (data not shown) of gel plugs without AM. They did not have any significant toxic effects.

3.4. *AM increased capillary density in gel plugs*

Microscopic observation of whole and sliced plugs revealed

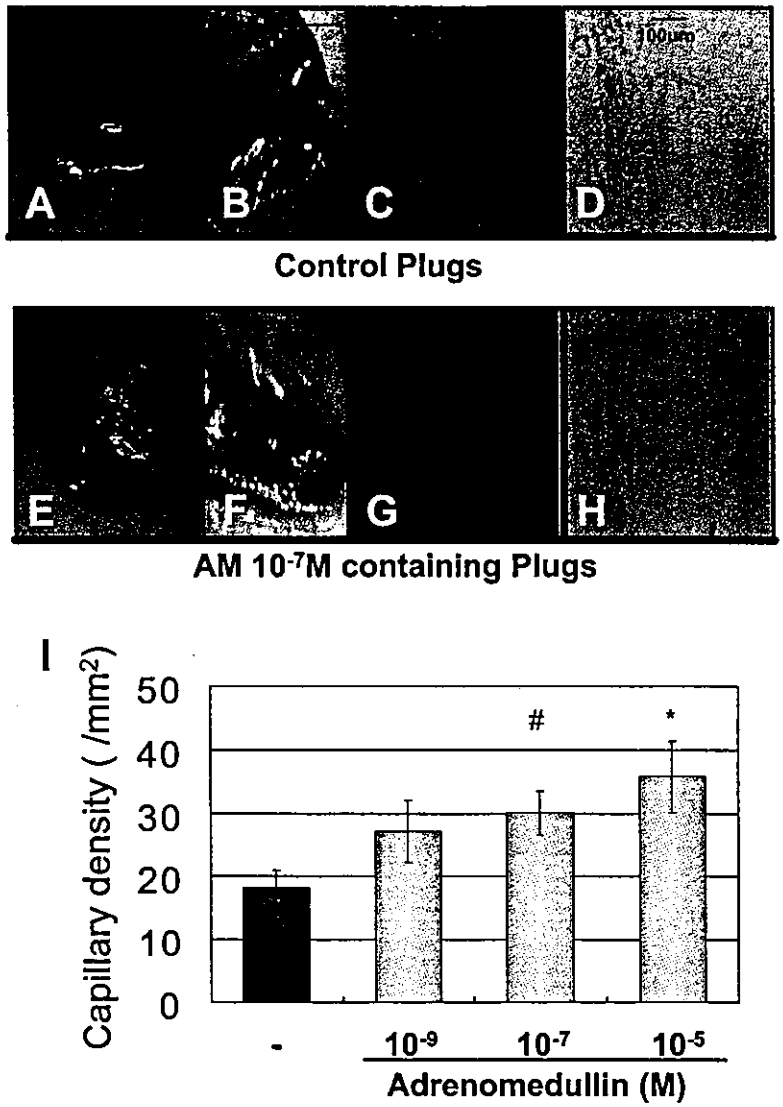

Fig. 4. Effect of AM on neo-vascularization in the gel plug. Gel plugs were harvested with underlying skin from mice on day 21 and angiogenic signs were microscopically examined. A–H: Representative images of a whole and sliced AM (10^{-7} mol/l)-containing plug (panels E and F) are shown, in comparison to the control plug (panels A and B). The plugs were stained with PECAM-1 to visualize neo-vessels. Immunochemically stained and fluorescent-labeled sections of an AM-containing plug (panels G and H) are shown, as compared to the control (panels C and D). The fluorescent-labeled sections were observed with a confocal microscope that can re-construct the 3D structure of small capillaries. I: Dose-dependent effect of AM on capillary density in the plugs determined by PECAM-1 immuno-reactivity on day 21. #: $P<0.05$; *: $P<0.01$ versus the control. $n=9$. Green: fluorescent-labeled PECAM-1 (panels C and G); brown: immunochemically stained PECAM-1 (panels D and H); arrows: neo-vessels in AM-containing plugs (panels F and H).

enhanced neo-vascularization in AM-containing plugs (Fig. 4E,F) compared to their control plugs (Fig. 4A,B). The capillary density estimated from PECAM-1 immuno-reactivity (Fig. 4D,H) was significantly and dose-dependently increased in AM-containing plugs (18.2 ± 2.8 per mm^2 in the control, 35.7 ± 5.7 per mm^2 in the 10^{-5} mol/l AM-containing plug on day 21; $P<0.01$ versus the control, $n=9$; Fig. 4I). We also confirmed increased capillary network in the AM-containing plug by observation with a confocal microscope that could visualize the 3D structure of capillaries of approximately 10 μm diameter (Fig. 4C,G).

4. Discussion

In this study, we showed that AM provokes endothelial Akt activation in a PKA- and PI3K-dependent manner and demonstrated that AM promotes endothelial regeneration in vitro and increases blood flow and capillary density in gel plugs in vivo through a PKA- and PI3K-dependent pathway.

AM-induced Akt activation in rat aortic tissues has been shown in a previous report [18]. In this study, we further confirmed that AM-induced Akt activation occurs in cultured endothelial cells. We also demonstrated that Akt is activated by the artificial wounds on HUVECs. Furthermore, we revealed that AM increases wound-induced Akt activation. Akt has been shown to regulate survival, migration, and nitric oxide production in endothelium [19]. In addition, constitutive Akt signaling in endothelium has been reported to be sufficient to promote angiogenesis in a rabbit hindlimb ischemia model [20]. Therefore, Akt activation in endothelium can be regarded as a key event in transduction of the angiogenic signal [21]. In the present study, AM-induced vascular regen-

Table 1
The effect of the AM antagonists and the inhibitors for PKA or PI3K on AM-induced endothelial regeneration

Treatment ($n=4$)	Re-endothelialized area (% control)	Treatment ($n=8$)	Re-endothelialized area (% control)
Control (FBS 0.5%)	100.0 ± 3.5	AM (10^{-8} mol/l)	132.6 ± 1.4[a]
+AM (22–52) (10^{-5} mol/l)	96.4 ± 5.4	+AM (22–52) (10^{-5} mol/l)	111.2 ± 7.4[b]
+CGRP (8–37) (10^{-5} mol/l)	103.3 ± 11.1	+CGRP (8–37) (10^{-5} mol/l)	119.8 ± 3.0[c]
+Rp-cAMP (10^{-5} mol/l)	104.0 ± 6.2	+Rp-cAMP (10^{-5} mol/l)	112.5 ± 11.7[b]
+PKA Inh. Peptide (5×10^{-7} mol/l)	101.7 ± 9.4	+PKA Inh. Peptide (5×10^{-7} mol/l)	113.0 ± 3.6[b]
+LY294002 (10^{-5} mol/l)	97.3 ± 14.7	+LY294002 (10^{-5} mol/l)	105.1 ± 6.6[b]
+Wortmannin (10^{-7} mol/l)	103.8 ± 13.1	+Wortmannin (10^{-7} mol/l)	103.0 ± 3.9[b]

Values are shown as mean ± S.E.M.
[a] $P<0.01$ versus the control.
[b] $P<0.01$ versus the AM (10^{-8} mol/l)-treated group without inhibitors.
[c] $P<0.05$ versus the AM (10^{-8} mol/l)-treated group without inhibitors.

Table 2
The effect of the AM antagonists and the inhibitors for PKA or PI3K on AM-induced augmentation of blood flow in gel plugs

Treatment ($n=4$)	Blood flow on day 21 (% control)	Treatment ($n=4$)	Blood flow on day 21 (% control)
Control	100.0 ± 0.0	AM (10^{-7} mol/l)	143.7 ± 5.5[a]
+AM (22–52) (10^{-4} mol/l)	101.1 ± 2.3	+AM (22–52) (10^{-4} mol/l)	104.1 ± 6.2[b]
+CGRP (8–37) (10^{-4} mol/l)	96.8 ± 10.1	+CGRP (8–37) (10^{-4} mol/l)	112.6 ± 3.7[b]
+Rp-cAMP (10^{-3} mol/l)	102.7 ± 11.7	+Rp-cAMP (10^{-3} mol/l)	113.2 ± 6.1[b]
+PKA Inh. Peptide (10^{-4} mol/l)	105.2 ± 6.1	+PKA Inh. Peptide (10^{-4} mol/l)	104.1 ± 9.8[b]
+LY294002 (10^{-3} mol/l)	100.1 ± 0.5	+LY294002 (10^{-3} mol/l)	109.3 ± 7.6[b]
+Wortmannin (10^{-5} mol/l)	101.2 ± 8.0	+Wortmannin (10^{-5} mol/l)	111.9 ± 7.4[b]

Values are shown as mean ± S.E.M.
[a] $P<0.01$ versus the control.
[b] $P<0.01$ versus AM (10^{-7} mol/l)-containing plugs without inhibitors.

eration both in vitro and in vivo was suppressed by PI3K inhibitors. Therefore, it is suggested that AM regulates neovascularization via enhancement of endothelial Akt activity following PI3K activation.

There are also several reports that imply the involvement of the cAMP/PKA cascade in vascular regeneration. However, whether PKA activation promotes or inhibits vascular regeneration is controversial [22,23]. In the present study, AM-induced vascular regeneration both in vitro and in vivo was significantly abrogated by the two PKA inhibitors, and 8-Br-cAMP simulated the effect of AM. Therefore, the cAMP/PKA cascade is supposed to have potency to promote vascular regeneration, at least in our experimental conditions. We also revealed that AM-induced Akt activation is suppressed by the inhibitors for not only PI3K but also for PKA. These results suggest the significance of the cAMP/PKA cascade on the regulation of Akt activity, which can induce vascular regeneration. The molecular mechanism in PKA-induced Akt activation is now under investigation.

In MATRIGEL plug assay, it has been reported that 10–100 times higher concentrations of substances than those used in cell culture experiments were required to exert enough influence in gel plugs [24,25]. Based on these previous reports, we planned to use higher concentrations of AM in MATRIGEL plug assay in vivo than in wound healing assay in vitro. As a result, the effective concentrations of AM were revealed to be 10^{-9}–10^{-7} mol/l in vitro and 10^{-7}–10^{-5} mol/l in vivo. The optimal concentrations of AM in vitro for cultured endothelial cells were similar to previous reports [26]. The difference between the effective concentrations in vitro and in vivo observed in our present study was also compatible with previous reports [24,25].

In conclusion, we demonstrated that AM provokes endothelial Akt activation and promotes vascular regeneration both in vitro and in vivo through a PKA- and PI3K-dependent pathway. These findings suggest the usefulness of AM as a new therapeutic agent for vascular injury, atherosclerotic diseases and tissue ischemia.

References

[1] Ross, R. (1993) Nature 362, 801–809.
[2] Carmeliet, P. (2000) Nat. Med. 6, 389–395.
[3] Suga, S., Nakao, K., Itoh, H., Komatsu, Y., Ogawa, Y., Hama, N. and Imura, H. (1992) J. Clin. Invest. 90, 1145–1149.
[4] Doi, K., Ikeda, T., Itoh, H., Ueyama, K., Hosoda, K., Ogawa, Y., Yamashita, J., Chun, T.H., Inoue, M., Masatsugu, K., Sawada, N., Fukunaga, Y., Saito, T., Sone, M., Yamahara, K., Kook, H., Komeda, M., Ueda, M. and Nakao, K. (2001) Arterioscler. Thromb. Vasc. Biol. 21, 930–936.
[5] Ohno, N., Itoh, H., Ikeda, T., Ueyama, K., Yamahara, K., Doi, K., Yamashita, J., Inoue, M., Masatsugu, K., Sawada, N., Fukunaga, Y., Sakaguchi, S., Sone, M., Yurugi, T., Kook, H., Komeda, M. and Nakao, K. (2002) Circulation 105, 1623–1626.
[6] Yamahara, K., Itoh, H., Chun, T.H., Ogawa, Y., Yamashita, J., Sawada, N., Fukunaga, Y., Sone, M., Yurugi-Kobayashi, T., Miyashita, K., Tsujimoto, H., Kook, H., Feil, R., Garbers, D.L., Hofmann, F. and Nakao, K. (2003) Proc. Natl. Acad. Sci. USA 100, 3404–3409.
[7] Kook, H., Itoh, H., Choi, B.S., Sawada, N., Doi, K., Hwang, T.J., Kim, K.K., Arai, H., Baik, Y.H. and Nakao, K. (2003) Am. J. Physiol. Heart Circ. Physiol. 284, 1388–1397.
[8] Kitamura, K., Kangawa, K., Kawamoto, M., Ichiki, Y., Nakamura, S., Matsuo, H. and Eto, T. (1993) Biochem. Biophys. Res. Commun. 192, 553–560.
[9] Eto, T. (2001) Peptides 22, 1693–1711.
[10] Shindo, T., Kurihara, H., Maemura, K., Kurihara, Y., Kuwaki, T., Izumida, T., Minamino, N., Ju, K.H., Morita, H., Oh-hashi, Y., Kumada, M., Kangawa, K., Nagai, R. and Yazaki, Y. (2000) Circulation 101, 2309–2316.
[11] Shindo, T., Kurihara, Y., Nishimatsu, H., Moriyama, N., Kakoki, M., Wang, Y., Imai, Y., Ebihara, A., Kuwaki, T., Ju, K.H., Minamino, N., Kangawa, K., Ishikawa, T., Fukuda, M., Akimoto, Y., Kawakami, H., Imai, T., Morita, H., Yazaki, Y., Nagai,

R., Hirata, Y. and Kurihara, H. (2001) Circulation 104, 1964–1971.
[12] Shimosawa, T., Shibagaki, Y., Ishibashi, K., Kitamura, K., Kangawa, K., Kato, S., Ando, K. and Fujita, T. (2002) Circulation 105, 106–111.
[13] Nakayama, M., Takahashi, K., Murakami, O., Murakami, H., Sasano, H., Shirato, K. and Shibahara, S. (1999) Clin. Sci. (Lond.) 97, 247–251.
[14] Cormier-Regard, S., Nguyen, S.V. and Claycomb, W.C. (1998) J. Biol. Chem. 273, 17787–17792.
[15] Miyashita, K., Itoh, H., Sawada, N., Fukunaga, Y., Sone, M., Yamahara, K., Yurugi, T. and Nakao, K. (2003) Hypertens. Res. 26, S93–8.
[16] Sawada, N., Itoh, H., Yamashita, J., Doi, K., Inoue, M., Masatsugu, K., Fukunaga, Y., Sakaguchi, S., Sone, M., Yamahara, K., Yurugi, T. and Nakao, K. (2001) Biochem. Biophys. Res. Commun. 280, 798–805.
[17] Passaniti, A., Taylor, R.M., Pili, R., Guo, Y., Long, P.V., Haney, J.A., Pauly, R.R., Grant, D.S. and Martin, G.R. (1992) Lab. Invest. 67, 519–528.
[18] Nishimatsu, H., Suzuki, E., Nagata, D., Moriyama, N., Satonaka, H., Walsh, K., Sata, M., Kangawa, K., Matsuo, H., Goto,.A., Kitamura, T. and Hirata, Y. (2001) Circ. Res. 89, 63–70.
[19] Morales-Ruiz, M., Fulton, D., Sowa, G., Languino, L.R., Fujio, Y., Walsh, K. and Sessa, W.C. (2000) Circ. Res. 86, 892–896.
[20] Kureishi, Y., Luo, Z., Shiojima, I., Bialik, A., Fulton, D., Lefer, D.J., Sessa, W.C. and Walsh, K. (2000) Nat. Med. 6, 1004–1010.
[21] Dimmeler, S. and Zeiher, A.M. (2000) Circ. Res. 86, 4–5.
[22] Amano, H., Ando, K., Minamida, S., Hayashi, I., Ogino, M., Yamashina, S., Yoshimura, H. and Majima, M. (2001) Jpn. J. Pharmacol. 87, 181–188.
[23] Kim, S., Bakre, M., Yin, H. and Varner, J.A. (2002) J. Clin. Invest. 110, 933–941.
[24] Wajih, N. and Sane, D.C. (2003) Blood 101, 1857–1863.
[25] Lee, M.J., Thangada, S., Claffey, K.P., Ancellin, N., Liu, C.H., Kluk, M., Volpi, M., Sha'afi, R.I. and Hla, T. (1999) Cell 99, 301–312.
[26] Michibata, H., Mukoyama, M., Tanaka, I., Suga, S., Nakagawa, M., Ishibashi, R., Goto, M., Akaji, K., Fujiwara, Y., Kiso, Y. and Nakao, K. (1998) Kidney Int. 53, 979–985.

Impaired adrenocorticotropic hormone response to bacterial endotoxin in mice deficient in prostaglandin E receptor EP1 and EP3 subtypes

Yoko Matsuoka*†, Tomoyuki Furuyashiki*, Haruhiko Bito*, Fumitaka Ushikubi*, Yasuhiro Tanaka*, Takuya Kobayashi*, Seiji Muro†, Noriko Satoh†, Tetsuro Kayahara‡, Mikito Higashi‡, Akira Mizoguchi‡, Hitoshi Shichi§, Yoshihiro Fukuda†, Kazuwa Nakao†, and Shuh Narumiya*¶

Departments of *Pharmacology and †Medicine and Clinical Science, Kyoto University Faculty of Medicine, Kyoto 606-8501, Japan; ‡Department of Anatomy, Mie University Faculty of Medicine, Tsu 514-8507, Japan; and §Department of Ophthalmology, Wayne State University School of Medicine, Detroit, MI 48201.

Edited by Shigetada Nakanishi, Kyoto University, Kyoto, Japan, and approved February 3, 2003 (received for review June 4, 2002)

Sickness evokes various neural responses, one of which is activation of the hypothalamo–pituitary–adrenal (HPA) axis. This response can be induced experimentally by injection of bacterial lipopolysaccharide (LPS) or inflammatory cytokines such as IL-1. Although prostaglandins (PGs) long have been implicated in LPS-induced HPA axis activation, the mechanism downstream of PGs remained unsettled. By using mice lacking each of the four PGE receptors (EP1–EP4) and an EP1-selective antagonist, ONO-8713, we showed that both EP1 and EP3 are required for adrenocorticotropic hormone release in response to LPS. Analysis of c-Fos expression as a marker for neuronal activity indicated that both EP1 and EP3 contribute to activation of neurons in the paraventricular nucleus of the hypothalamus (PVN). This analysis also revealed that EP1, but not EP3, is involved in LPS-induced activation of the central nucleus of the amygdala. EP1 immunostaining in the PVN revealed its localization at synapses on corticotropin-releasing hormone-containing neurons. These findings suggest that EP1- and EP3-mediated neuronal pathways converge at corticotropin-releasing hormone-containing neurons in the PVN to induce HPA axis activation upon sickness.

During sickness, various responses of the CNS are evoked in animals through the immune–brain interaction, one prominent example being the activation of the hypothalamo–pituitary–adrenal (HPA) axis (1, 2). In this response, a population of parvocellular neurons in the paraventricular nucleus of the hypothalamus (PVN) are activated to secrete corticotropin-releasing hormone (CRH), which then triggers the release of adrenocorticotropic hormone (ACTH) from the pituitary to the plasma, and the latter finally stimulates the secretion of corticosteroids (2). This neuroendocrine cascade is a primordial step in host defense mechanism that is mobilized upon exposure to a large variety of stresses (2–4). Activation of the HPA axis that occurs during systemic diseases can be mimicked experimentally by injection of bacterial endotoxin, lipopolysaccharide (LPS), or inflammatory cytokines such as IL-1. By using these models, the mechanism of the sickness-induced HPA axis activation has been studied extensively, and these studies suggest the involvement of prostaglandins (PGs) in the initiation of this neuroendocrine cascade.

PGs are lipid mediators produced from arachidonic acid by the sequential actions of cyclooxygenases (COX) and respective synthases, and they include PGD_2, PGE_2, $PGF_{2\alpha}$, PGI_2, and thromboxane A_2 (5). They are released from cells in response to a variety of physiological and pathological stimuli and act in the vicinity of their site of synthesis. Roles of PGs have been studied by examining actions of either exogenously applied PGs or nonsteroidal antiinflammatory drugs (NSAIDs), such as indomethacin, that block the production of PGs by inhibiting COX. Indeed, in previous experiments the HPA axis activation by either LPS or IL-1 was attenuated by pretreatment of animals with NSAIDs, and PGE_2 injected centrally into the brain induced PVN activation and ACTH release (6–11). However, the inhibition by NSAIDs was not always complete, was often short-lived, and was sometimes inconsistent (2). In addition, no systematic effort to pinpoint the identity of the critical PG involved in this process has yet been performed. Consequently, the physiological significance of PGs in HPA axis regulation has remained obscure. This situation appears to be mainly because of the lack of appropriate experimental tools to dissect various PG-mediated steps in the CNS.

PGs exert their effects through interaction with eight types and subtypes of cell surface receptors. They include PGD receptor (DP), four subtypes of PGE receptor (EP1, EP2, EP3, and EP4), PGF receptor (FP), PGI receptor (IP), and thromboxane A receptor (TP). All of these receptors are G protein-coupled receptors with seven transmembrane domains (5). We have disrupted genes for these receptors individually in mice and analyzed phenotypes of the resulting knockout animals (12–17). Using these mice, we showed previously that the PGE receptor EP3 in the brain plays a critical role in the generation of febrile response to LPS and IL-1β (15). Because LPS and IL-1 evoke activation of the HPA axis together with fever under these conditions, we suspected that PGE_2–EP3-mediated mechanism also might underlie elicitation of other CNS responses to sickness. Our results suggest that LPS-induced ACTH release indeed is defective in EP3-deficient mice. However, we found that this ACTH response also is defective in EP1-deficient mice. Furthermore, both EP1 and EP3 play a critical role in regulating the PVN in the HPA axis activation.

Materials and Methods

Mice. Mice lacking EP1, EP2, EP3, or EP4 receptor were generated as described (14–16). With the exception of $EP4^{-/-}$ mice, each mutant line was backcrossed for more than five generations into C57BL/6CrSlc (Japan SLC, Hamamatsu, Japan). Because most $EP4^{-/-}$ mice die postnatally (14), survivors of the F_2 progenies of $EP4^{-/-}$ mice in the mixed genetic background of 129/Ola × C57BL/6 were intercrossed and the resultant male survivors were used. All experiments were performed according to the guidelines for animal experiments of Kyoto University.

Measurement of LPS-Induced ACTH Release. Before each experiment, 8- to 12-week-old male mice were caged individually for 3

This paper was submitted directly (Track II) to the PNAS office.

Abbreviations: ACTH, adrenocorticotropic hormone; CeA, central nucleus of the amygdala; COX, cyclooxygenase; CRH, corticotropin-releasing hormone; HPA, hypothalamo–pituitary–adrenal; IR, immunoreactivity; LPS, lipopolysaccharide; mPGES-1, microsomal prostaglandin E synthase; NSAIDs, nonsteroidal antiinflammatory drugs; NTS, nucleus of the solitary tract; PG, prostaglandin; PVN, paraventricular nucleus of the hypothalamus; VLM, ventrolateral medulla.

¶To whom correspondence should be addressed. E-mail: snaru@mfour.med.kyoto-u.ac.jp.

www.pnas.org/cgi/doi/10.1073/pnas.0633341100

days under standard conditions (12-h light/12-h dark cycle; light on between 0900 and 2100), with free access to chow and water, and handled daily. Each mouse was injected i.p. with 0.11 ml of an LPS (*Escherichia coli* O26:B6) suspension (0.02 mg/ml) and killed by decapitation. Plasma ACTH concentration was determined with an immunoradiometric assay kit as described (18). A volume of 0.22 ml of indomethacin solution (5 mg/ml in Dulbecco's PBS) or vehicle was injected i.p. 15 min before LPS injection. An EP1 antagonist, ONO-8713 (19), kindly provided by Ono Pharmaceutical (Osaka), was dissolved at a concentration of 10 mg/ml in 1 M NaOH containing 5% glucose. The solution was adjusted to pH 9.0 with 5 M HCl and then diluted 10-fold with PBS before i.p injection of 0.22 ml 60 min before LPS injection.

Immunohistochemistry. For immunostainings of c-Fos and CRH, mice were killed by transcardiac perfusion with 0.1 M phosphate buffer containing 4% paraformaldehyde. Coronal brain sections of 30-μm thickness were prepared, and c-Fos immunoreactivity (Fos-IR) was detected by using a rabbit polyclonal anti-c-Fos antibody (1:2,000 dilution, Ab-5; Oncogene Science) and a Vectastain ABC-PO kit (Vector Laboratories), as described (20). Two sections with the highest numbers of Fos-IR-positive cells were identified for each region, and the mean number was taken as the representative score for each mouse. For double immunostaining, sections were incubated with the anti-c-Fos and guinea pig anti-CRH (1:200 dilution, T-5007; Peninsula Laboratories) antibodies. Signals were detected with Alexa 488-labeled anti-rabbit and Alexa 594-labeled anti-guinea pig IgG antibodies (1:200 dilution; Molecular Probes), respectively.

Immunostaining of COX-1, COX-2, and microsomal PGE synthase-1 (mPGES-1) was carried out as described (21, 22) by using mouse anti-COX-1 (1:500 dilution, 160110; Cayman Chemical, Ann Arbor, MI), goat anti-COX-1 (1:1,000 dilution, sc-1752, Lot D-208; Santa Cruz Biotechnology), rabbit anti-mouse COX-2 (1:1,000 dilution, 160126; Cayman Chemical), rabbit anti-mPGES-1 (1:1,500 dilution, 160140; Cayman Chemical), or guinea pig anti-mPGES-1 (1:500 dilution; ref. 23) antibodies. COX-1-IR was detected by Alexa 488-labeled anti-mouse and/or Alexa 594-labeled anti-goat IgG antibodies (1:500 dilution; Molecular Probes). Signals for COX-2 and mPGES-1 were detected with a biotinylated anti-rabbit IgG antibody (Jackson ImmunoResearch) followed by Alexa 488- or Alexa 594-labeled streptavidin (Molecular Probes) or with Alexa 488-labeled anti-guinea pig IgG antibody. The specificity of each signal was confirmed by the use of two independent antibodies for COX-1 and mPGES-1 or by loss of COX-2-IR on brain sections from COX-2$^{-/-}$ mice.

For immunostaining of EP1, synaptophysin, and CRH, fresh brains were frozen, cut coronally at a thickness of 10 μm, then serially treated with 95% ethanol at −20°C for 30 min and 100% acetone for 3 min at room temperature. They were incubated with rabbit anti-EP1 (1:400 dilution) (24), mouse anti-synaptophysin (1:50 dilution, 61012; Progen, Heidelberg), and/or guinea pig anti-CRH antibodies. Signals were detected with fluorescein- and/or Texas red-labeled secondary antibodies (1:200 dilution). All fluorescent images were acquired with laser-scanning confocal microscopy [MRC1024 (Bio-Rad) or LSM510 (Zeiss)].

Semiquantitative RT-PCR. Mice were injected with LPS (2.5 mg/kg) i.p. and killed by decapitation 3 h later. The hypothalamus was isolated as defined (25) and homogenized within 3 min after decapitation. Total RNA was extracted by using TRIzol solution (Invitrogen) and subjected to semiquantitative RT-PCR by using Light-Cycler (Roche Diagnostics) as described (26). Primers and fluorescent probes for mouse c-fos and GAPDH mRNA were obtained from Nihon Gene Research Laboratories (Sendai, Japan). The amount of c-Fos mRNA was normalized to that of GAPDH mRNA from the same cDNA sample and is shown as the ratio to the value in vehicle-treated wild-type mice.

Statistical Analyses. Data are shown as means ± SEM. Comparison of two groups was analyzed by Student's *t* test. For comparison of more than two groups with comparable variances, one-way ANOVA was performed first. Then, either Dunnett's or Tukey's test was used to evaluate pairwise group difference. If the variances of the groups were significantly different, a Kruskal–Wallis test followed by Dunn's test was used for nonparametric comparisons. The analyses were performed with the use of PRISM 3.0 software (GraphPad, San Diego).

Results

LPS-Induced HPA Axis Activation Is Impaired in EP1$^{-/-}$ and EP3$^{-/-}$ Mice. Given the previous inconsistent effects of NSAIDs on ACTH release (see ref. 2), we first examined the time course of inhibition of ACTH response to LPS by indomethacin. We measured the plasma ACTH concentration at various times after LPS injection (0.1 mg/kg i.p.) without (vehicle/LPS) or with (IND/LPS) indomethacin administered (50 mg/kg i.p.) 15 min before LPS injection (Fig. 1*A*). The ACTH concentration in the vehicle/LPS group significantly increased at 60 min, peaked at 120 min, and decreased but still remained higher than the control at 180 min, whereas no change was observed in control mice injected with saline. Indomethacin treatment before LPS challenge abolished the ACTH increase at 60 and 180 min. The peak response at 120 min was not affected significantly, although the value at 120 min also tended to be lower than that for the vehicle/LPS group. These results indicate that the LPS-induced ACTH release in mice is composed of two components: an indomethacin-sensitive component that was apparent at all time points and an indomethacin-resistant component that was transient and peaked at 120 min. A similar NSAID effect on LPS-induced ACTH release was reported previously (27).

We next examined whether LPS induces the release of ACTH in mice deficient in any one of the four EP subtypes. The plasma ACTH level from the knockout and wild-type mice was measured at 1 h after LPS challenge. At this time point, EP2$^{-/-}$ and EP4$^{-/-}$ mice exhibited an increase in ACTH concentration similar to that apparent in wild-type mice (Fig. 1*B*). However, no increase in ACTH concentration was found in either EP1$^{-/-}$ or EP3$^{-/-}$ mice. As found in the indomethacin-treated animals, both EP1$^{-/-}$ and EP3$^{-/-}$ mice elicited a peak of ACTH release at 2 h after LPS injection, but neither of them showed the increase at 3 h (data not shown). The impairment in EP1$^{-/-}$ and EP3$^{-/-}$ mice was confirmed by comparing the responses among littermates born from EP1- or EP3-heterozygous mice (data not shown). The role of EP1 in ACTH release was confirmed further pharmacologically by the use of a highly selective EP1 antagonist, ONO-8713 (19) (Fig. 1*C*). The treatment with this antagonist suppressed the LPS-induced ACTH release in wild-type mice, whereas it did not affect the febrile response, an EP3-mediated process (15) (Fig. 1 *D* and *E*). These results suggest that both EP1 and EP3 play a crucial role in mediating LPS-induced ACTH release and, further, that EP1 participates in this response by a process independent of EP3-mediated febrile response.

Defective LPS-Induced c-Fos Expression in Neurons of EP1$^{-/-}$ and EP3$^{-/-}$ Mice. The loss of LPS-induced ACTH release by EP1 or EP3 deficiency described above could be attributed to defect(s) either in PVN activation or in CRH action on the pituitary. To examine which step is affected by EP1 or EP3 deficiency, we determined LPS-induced c-fos expression in the PVN and the pituitary of wild-type, EP1$^{-/-}$, and EP3$^{-/-}$ mice. Because substantial Fos-IR was detected not at 60 min but at 120 min after

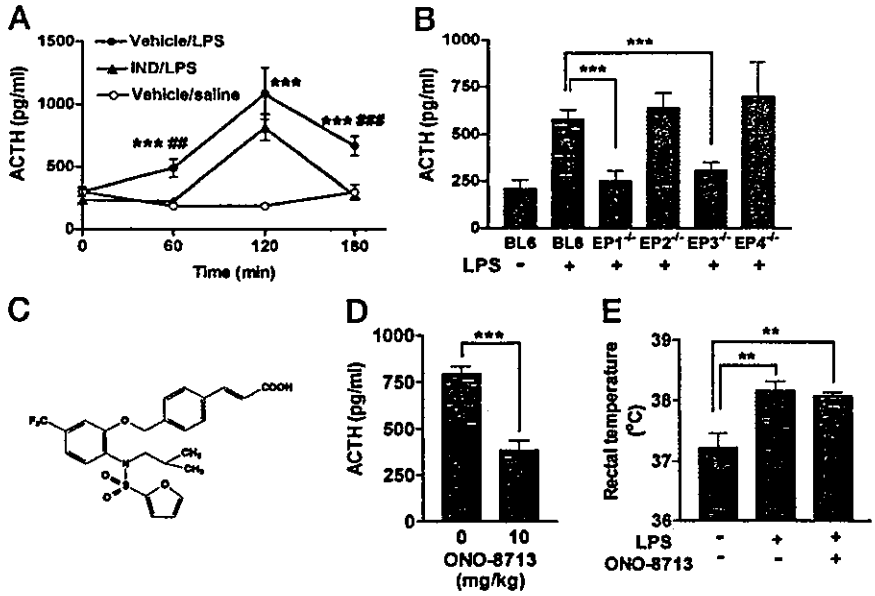

Fig. 1. Impaired LPS-induced ACTH release in EP1$^{-/-}$ and EP3$^{-/-}$ mice. (*A*) Inhibition of LPS-induced ACTH release by indomethacin. Time course of the plasma ACTH concentration after injection of LPS (0.1 mg/kg i.p.) or saline is shown in the absence (Vehicle) or presence (IND) of indomethacin pretreatment (nine mice per group). ○, Vehicle + saline; ●, vehicle + LPS; ▲, indomethacin + LPS. ***, $P < 0.001$ vs. Vehicle/saline; ##, $P < 0.01$; ###, $P < 0.001$ vs. IND/LPS. (*B*) Effects of EP deficiency on LPS-induced ACTH release. Wild-type mice were injected with either saline ($n = 6$) or LPS ($n = 9$). EP1$^{-/-}$ ($n = 9$), EP2$^{-/-}$ ($n = 9$), EP3$^{-/-}$ ($n = 9$), and EP4$^{-/-}$ ($n = 5$) mice were injected with LPS. Their plasma ACTH concentrations were measured after 1 h. ***, $P < 0.001$. (*C*) Structure of ONO-8713. (*D*) Inhibition of LPS-induced ACTH release by ONO-8713 ($n = 6$ each). ***, $P < 0.001$. (*E*) Effect of ONO-8713 on LPS-induced increase in body temperature ($n = 6$ each). **, $P < 0.01$.

LPS injection, the numbers of positive cells were determined at the latter time point. Wild-type, EP1$^{-/-}$, and EP3$^{-/-}$ mice showed similar numbers of Fos-IR-positive cells in the PVN with no significant difference among the groups (Fig. 2*A*). No difference was found, either, in the pituitary among the three lines of mice (data not shown). Although these results appeared to suggest that neither EP1 nor EP3 deficiency affects neuronal activation in these areas, we suspected that either deficiency did affect the activation but only to the level that was sufficient to blunt ACTH release but not sufficient to decrease the number of Fos-IR-positive cells. It is known that the level of c-Fos has a rather complex relationship with neuronal firing (28). Because both EP1 and EP3 are involved in ACTH release, it is possible that inhibition of one of these receptors leaves the pathway

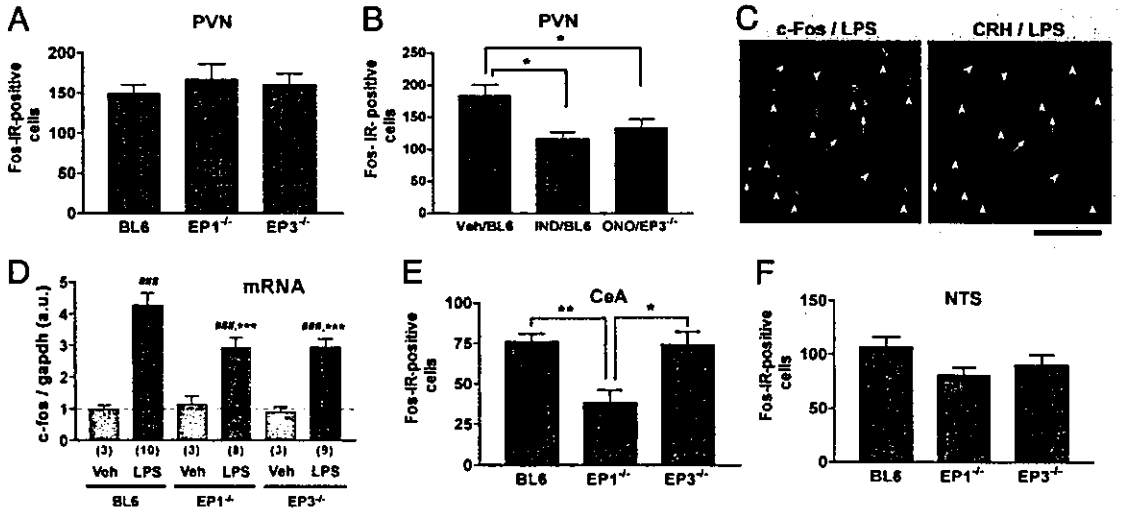

Fig. 2. LPS-induced c-Fos response in wild-type, EP1$^{-/-}$, and EP3$^{-/-}$ mice. (*A*) Fos-IR response in the PVN. The numbers of Fos-IR-positive cells in the PVN of each group of mice are shown ($n = 7$ each). (*B*) Effects of indomethacin and ONO-8713 on Fos-IR response in the PVN. Wild-type mice (BL6) treated with either vehicle (Veh; $n = 7$) or indomethacin (IND; $n = 7$) or EP3$^{-/-}$ mice treated with ONO-8713 (ONO; $n = 9$) were challenged with LPS and analyzed for c-Fos response. *, $P < 0.05$ vs. vehicle-treated wild-type mice. (*C*) Double immunostaining of c-Fos and CRH in the PVN of LPS-treated wild-type mice. Arrowheads and arrows show Fos-IR-positive neurons with or without CRH-IR, respectively. (Bar = 50 μm.) (*D*) Induction of c-fos mRNA. Wild-type (BL6), EP1$^{-/-}$, and EP3$^{-/-}$ mice (the numbers appear in parentheses) were injected with either vehicle or LPS, and c-fos mRNA in the hypothalamus was quantified by RT-PCR. The amount of c-fos mRNA was normalized to that of GAPDH mRNA. ###, $P < 0.001$ vs. vehicle-treated mice of the respective genotype; ***, $P < 0.001$ vs. LPS-treated wild-type mice. (*E*) Fos-IR response in the central nucleus of the amygdala (CeA) ($n = 7$ each). *, $P < 0.05$ and **, $P < 0.01$ vs. EP3$^{-/-}$ and wild-type mice, respectively. (*F*) Fos-IR response in the nucleus of the solitary tract (NTS). The numbers of wild-type, EP1$^{-/-}$, and EP3$^{-/-}$ mice are 13, 14, and 8, respectively.